

NASA Technical Memorandum 4499

1N-02

180072

29P

Space Shuttle
Hypersonic
Aerodynamic and
Aerothermodynamic
Flight Research and
the Comparison to
Ground Test Results

Kenneth W. Iliff and Mary F. Shafer

JUNE 1993

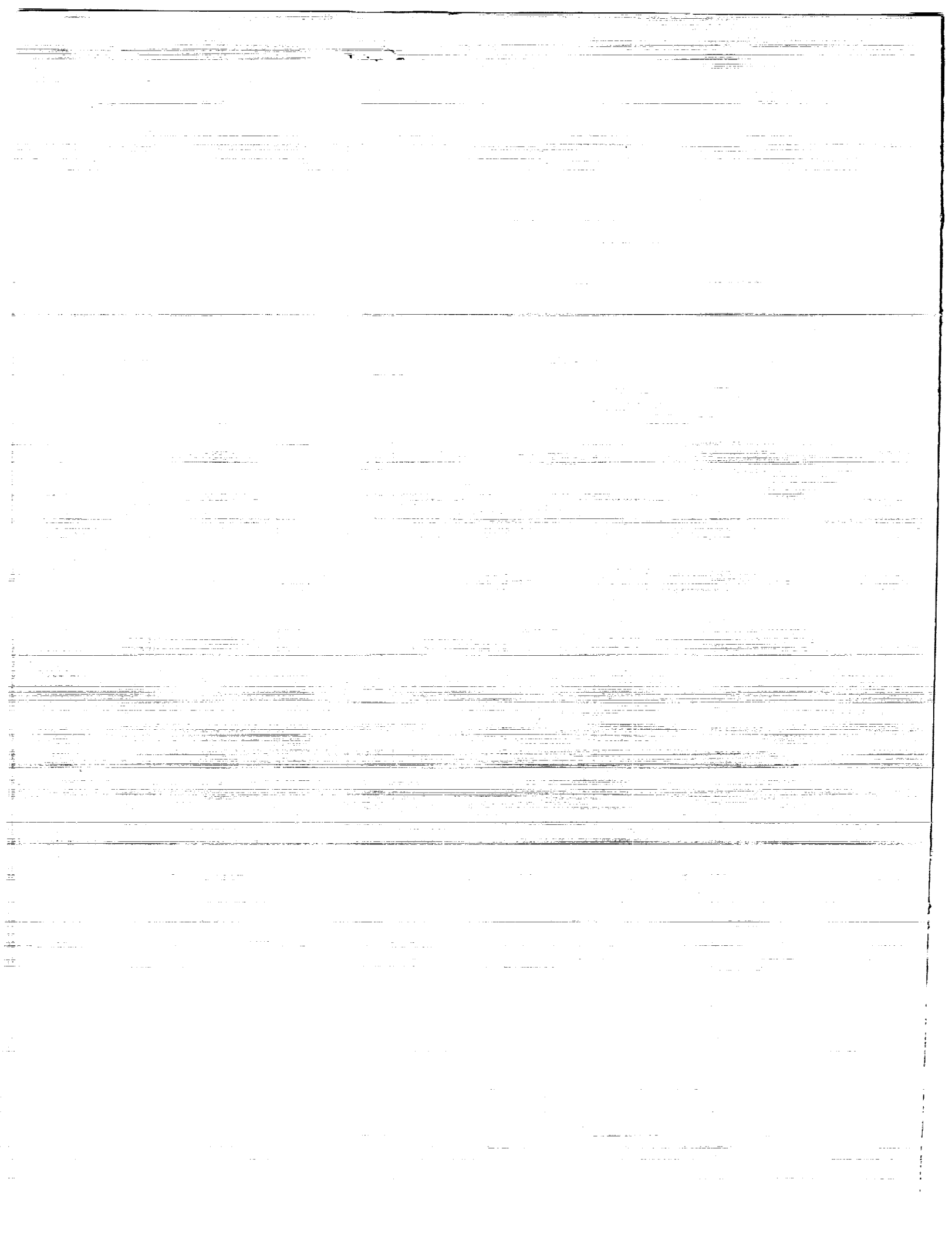
(NASA-TM-4499) SPACE SHUTTLE
HYPERSONIC AERODYNAMIC AND
AEROTHERMODYNAMIC FLIGHT RESEARCH
AND THE COMPARISON TO GROUND TEST
RESULTS (NASA) 29 p

N94-10820

Unclass

H1/02 0180072





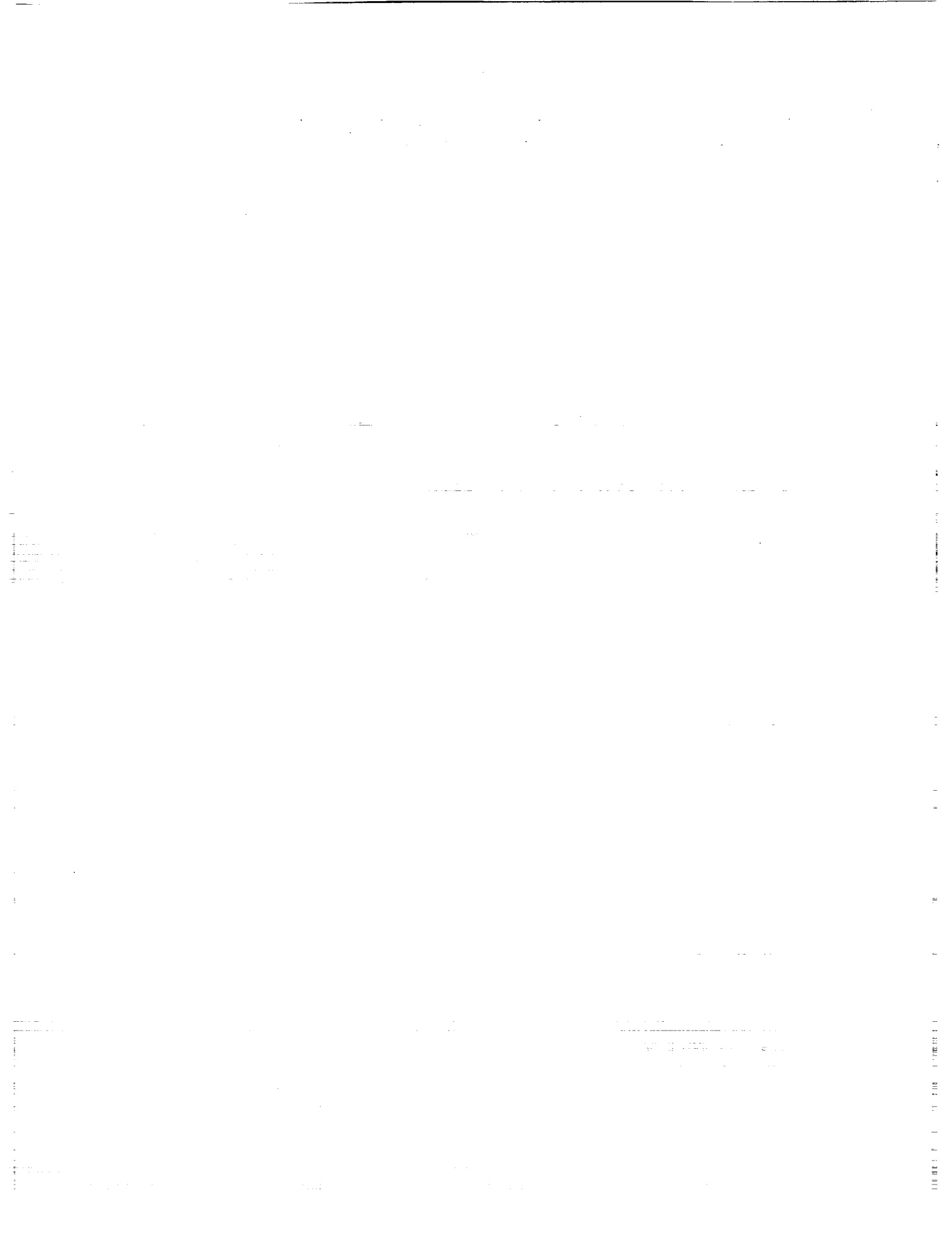
NASA Technical Memorandum 4499

Space Shuttle Hypersonic Aerodynamic and Aerothermodynamic Flight Research and the Comparison to Ground Test Results

Kenneth W. Iliff and Mary F. Shafer
*Dryden Flight Research Facility
Edwards, California*



National Aeronautics and
Space Administration
Office of Management
Scientific and Technical
Information Program
1993



SPACE SHUTTLE HYPERSONIC AERODYNAMIC AND AEROTHERMODYNAMIC FLIGHT RESEARCH AND THE COMPARISON TO GROUND TEST RESULTS

Kenneth W. Iliff* and Mary F. Shafer**
 NASA Dryden Flight Research Facility
 P.O. Box 273
 Edwards, California 93523-0273

Abstract

Aerodynamic and aerothermodynamic comparisons between flight and ground test for the Space Shuttle at hypersonic speeds are discussed. All of the comparisons are taken from papers published by researchers active in the Space Shuttle program. The aerodynamic comparisons include stability and control derivatives, center-of-pressure location, and reaction control jet interaction. Comparisons are also discussed for various forms of heating, including catalytic, boundary layer, top centerline, side fuselage, OMS pod, wing leading edge, and shock interaction. The jet interaction and center-of-pressure location flight values exceeded not only the predictions but also the uncertainties of the predictions. Predictions were significantly exceeded for the heating caused by the vortex impingement on the OMS pods and for heating caused by the wing leading-edge shock interaction.

Nomenclature

Acronyms

ACIP	Aerodynamic Coefficient Instrumentation Package
ADDB	aerodynamic design data book orbiter vehicle STS-1
BET	Best Estimated Trajectory
BF	body flap
CP	center of pressure
EST	estimated
HRSI	high-temperature reusable surface insulation

IMU	inertial measurement unit
NASP	National Aero-Space Plane
NOM	nominal
OEX	orbiter experiments
OI	operational instrumentation
OMS	orbital maneuvering system
POPU	push-over-pull-up or pull-up-push-over
RCG	reaction-cured glass
RCC	reinforced carbon-carbon
RCS	reaction control system
REYN	free-stream Reynolds number
SHTNEQ	viscous-shock-layer code
STS	Space Transportation System, prefix for flight number
TPS	thermal protection system
T/C	thermocouple

Symbols

C'_{∞}	free-stream proportionality factor for the linear viscosity-temperature relationship
$C_{l_{\beta}}$	coefficient of rolling moment due to angle of sideslip, per deg
$C_{l_{\delta_a}}$	coefficient of rolling moment due to aileron deflection, per deg
C_{m_0}	coefficient of pitching moment bias
$C_{m_{\alpha}}$	coefficient of pitching moment due to angle of attack, per deg
$C_{m_{BF}}$	coefficient of pitching moment due to body flap deflection, per deg
$C_{m_{\delta_e}}$	coefficient of pitching moment due to elevator deflection, per deg

*Senior Staff Scientist, Fellow, AIAA

**Aerospace Engineer, Associate Fellow, AIAA

Copyright ©1992 by the American Institute of Aeronautics and Astronautics, Inc. No copyright is asserted in the United States under Title 17, U.S. Code. The U.S. Government has a royalty-free license to exercise all rights under the copyright claimed herein for Governmental purposes. All other rights are reserved by the copyright owner.

$C_{n\beta}$	coefficient of yawing moment due to angle of sideslip, per deg
$C_{n\delta_a}$	coefficient of yawing moment due to aileron deflection, per deg
K	height of misaligned tiles, in.
L_{YJ}	rolling moment due to yaw jet, ft-lbf per jet
M	Mach number
M_∞	free-stream Mach number
$M_\infty/\sqrt{R_\infty}$	viscous interaction parameter
\dot{M}_j/\dot{M}_∞	jet-to-free-stream mass flow ratio
R_∞	free-stream Reynolds number
Re_∞	free-stream Reynolds number
Re_k	Reynolds number at top of misaligned tiles
$R_{NS,L}$	Reynolds number evaluated behind a normal shock based on orbiter characteristic length
$R_{NS,L}^{0.2}$	$R_{NS,L}$ at $X/L = 0.2$
S	surface length, in.
St	Stanton number
T	temperature, deg F
\bar{T}	normalized surface temperature
U_∞	free-stream velocity, km/sec
\bar{V}_∞	viscous interaction parameter, $M_\infty \sqrt{\frac{C_{f_w}}{Re}}$
X	axial coordinate, in.
X, x	axial distance from nose of orbiter, m
$X/L, x/L$	nondimensional body length
$X_{CP/LB}$	center of pressure in body length
Y	spanwise coordinate, in.
a_n	normal acceleration, g
h	altitude, ft
k_w	surface catalytic recombination rate constant, cm/sec
k_{wO}	k_w for oxygen, cm/sec
k_{wN}	k_w for nitrogen, cm/sec
q	convective heat-transfer rate, Btu/ft ² -sec
q	pitch rate, deg/sec
q_c	convective heating rate, Btu/ft ² -sec
\dot{q}	heat-transfer rate, kW/m ²
s/L	side fuselage thermocouple location
t	time, sec

α	angle of attack, deg
β	angle of sideslip, deg
δ_a	aileron (differential elevon) deflection, deg
δ_e	elevator (symmetric elevon) deflection, deg
ϵ_{TH}	total hemispherical emittance
ρ_∞	free-stream density, kg/m ³
θ	pitch angle, deg

Introduction

A continuing interest in advancing the understanding of aerodynamic phenomena using intensive comparisons between flight and ground test data exists. This interest started when the Wright brothers first demonstrated powered flight 89 yr ago after using their wind tunnel to make predictions. These continuing comparisons have resulted in the steady advancement of aerodynamics (new phenomenology and modified theory) by forcing *agreement* between ground and flight results. This procedure has resulted in more advanced flight vehicles with ever-increasing economy, improved safety, and better performance.

Hypersonic flight was demonstrated with the Project Mercury and X-15 aircraft (North American Aviation, Los Angeles, California) flight programs in the early 1960's. In the 1960's, several programs successfully generated aerothermodynamic flight data to improve the understanding and interpretation of theoretical and ground test results. The ASSET and PRIME programs were flown in the early and mid-1960's and provided aerothermodynamic flight data for ablative and metallic thermal protection system (TPS) concepts. The Apollo 4, FIRE I, and FIRE II programs provided flight data to validate predictions from theoretical radiation models and arc-jet ground test results in support of the return from lunar and planetary missions.¹⁻² The single-flight Reentry F vehicle was also flown in the 1960's when it returned the benchmark data still used today for hypersonic boundary-layer transition predictions at Mach numbers (M) up to 20 and altitudes (h) down to 80,000 ft.³

The X-15 research program was flown throughout the 1960's.⁴⁻⁷ This aircraft returned benchmark hypersonic data for aircraft performance, stability and control, materials, shock interaction, hypersonic turbulent boundary layer, skin friction, reaction control jets, aerodynamic heating, and heat transfer.

The Sandia National Laboratory (Albuquerque, New Mexico) vehicles provided much of the aerothermodynamic data obtained during the 1970's and 1980's.⁸ These data have provided new insights into the understanding and modification of existing theory and

ground test results. Currently, the Space Shuttle and the Pegasus vehicle (Orbital Sciences Corporation, Fairfax, Virginia) provide aerothermodynamic flight data for correlation with ground test results.⁹⁻¹²

This paper discusses the aerodynamic and aerothermodynamic comparisons between hypersonic flight and ground test results for the Space Shuttle.

Reusability and the Space Shuttle

The Space Shuttle brought to light many important issues that must be understood to make economically viable and fully reusable spacecraft a reality. Processes need to be developed that ensure a steady evolution of spacecraft which can be operated in a manner similar to aircraft.

Processes have been developed to go from subsonic to transonic to supersonic flight and for hypersonic glide vehicles. Future processes will be developed to include hypersonic airbreathing vehicles. For example, simulation and ground test facilities led to the X-15 aircraft. Results from this flight experiment, combined with the results from entry capsules, reduced the technical uncertainty associated with hypersonic glide vehicles. This reduction of technical uncertainty, including 46,000 hr of wind-tunnel testing,¹³ enabled engineers to propose and successfully fly the Space Shuttle, the first generation of operational vehicles that can return from space and fly like an airplane.¹⁴ The results from these flights will help engineers design more advanced vehicles because of further reductions in technical uncertainty.

In particular, information acquired in flying the Space Shuttle demonstrates the difficulty in designing and building an economical, reusable launch vehicle. The Space Shuttle must essentially be recertified after every flight even though the vehicle was designed to be the first reusable space vehicle.

The main argument for reusable spacecraft is an economic one, the same reason that expendable transportation systems have not been developed for other purposes. In addition to squandering limited resources, such a philosophy for launch vehicles would end with space cluttered with expendable vehicles, rendering subsequent flight unnecessarily hazardous. Consider what modern air transport would be like if the airlines disposed of aircraft after a single flight. Rather, aircraft were designed to be placed in service and used repeatedly even as manufactures sought to produce better and more advanced aircraft. The long-term cost-benefits of this policy are reflected in the price of modern air travel.

While current airliner technology is well understood and well developed, two major technological areas must be mastered before routine, economical flight to any desired orbit can be achieved. The first is development of a fully reusable rocket (ultimately single-stage-to-orbit), and the second is the assessment of the viability of airbreathing scramjet technology. The first area will provide economy in routine spaceflight, while the flexibility of an efficient scramjet will make any orbit accessible (decoupling the desired orbit from the launch site).

Aerodynamic and aerothermodynamic lessons learned in testing and flying the Space Shuttle have provided valuable information that will ease the development of single-stage-to-orbit vehicles. In addition to these issues, it is also necessary to examine the economic and operational issues of going to space routinely. True reusability characterized by certification similar to that of an airliner rather than recertification after every flight is a necessary first step. In addition, such key reusability technologies as reusable cryogenic materials and lightweight, durable thermal protection systems need to be developed and evaluated on the ground and in flight.

The quickest way to examine both economic and technological issues may be an experimental aircraft approach. A vehicle similar to the Space Shuttle or lifting-body would provide a robust testbed and can be built immediately with off-the-shelf, proven aircraft and system technologies. Using a configuration similar to an aircraft, including horizontal vehicle processing and fault-tolerant approaches, should result in an understanding of the key processes necessary for an economical, reusable spacecraft.

The second major area is developing an operational scramjet engine. The turbojet engine is over 50 yr old and has been developed incrementally through scores of new, flight-proven designs to attain the highly efficient turbojets of today. The supersonic combustion theory that is required for a useful scramjet is over 35 yr old, and the concepts have been tested in wind tunnels for over 20 yr. However, they must be proven in flight before a scramjet-powered booster becomes viable. Here, too, a rocket-powered testbed vehicle based on off-the-shelf components could carry various candidate scramjet modules into flight. Air-launching the rocket-powered testbed would simplify the design and such a testbed could fly to Mach numbers about 10 at desired altitudes for the testing of the interchangeable scramjet modules. Data acquired in such tests would, of course, be used to define subsequent modules. A specialized rocket-powered vehicle could be used to

verify the basic scramjet phenomenology with a few flight tests that gather data at speeds between Mach 10 and 20.

This section highlighted issues that the Space Shuttle has shown need to be addressed before an economical and reusable spacecraft can be realized. The next section describes what a valuable aerodynamic and aerothermodynamic research vehicle the Space Shuttle has been.

Space Shuttle Data Presentation

Since 1981 the Space Shuttle (Fig. 1) has provided many opportunities to compare ground tests with flight tests for aerodynamic and aerothermodynamic data. Many of these comparisons are discussed in the literature. This paper summarizes some of the more significant results published to date. The comparison is primarily from the ground test perspective. In a field as diverse as aerothermodynamics, these comparisons cover a wide variety of phenomena and their accompanying nomenclature.

Because of length constraints on this paper, the data comparisons between ground tests and flight tests are taken exactly as they appeared in the original referenced document. Unfortunately, full interpretations of the results may not be evident to the nonspecialist, so it is left to the reader to go to the referenced documents for more complete treatment of the phenomena. Statements from the referenced documents are frequently taken nearly verbatim to ensure that they are consistent with the discussion of the figures and faithfully represent the conclusions of the referenced authors. The intent here is to expose the reader to the variety of meaningful aerothermodynamic ground and flight test results to show the way flight data (sometimes incidental) can be used to bring to light new interpretations of phenomena.

The flight data that have been used were from the available Space Shuttle instrumentation. A complete description of this instrumentation is given in Ref. 15. This reference discusses the specific orbiter experiments (OEX) that were performed to enhance the understanding of the aerothermodynamic phenomena as well as the orbiter operational instrumentation (OI) that is used on all Space Shuttle flights.

Space Shuttle Hypersonic Aerodynamics

Many interesting aerodynamic phenomena were investigated on the Space Shuttle. The most interesting in terms of the vehicle dynamics are discussed in this section.

Stability and Control Derivatives

The stability and control derivatives of the Space Shuttle were examined extensively in wind-tunnel testing and in approach and landing tests. The wind-tunnel data were also incorporated into simulators and used in the design of the flight control system. No matter how carefully wind-tunnel tests are performed, discrepancies sometimes occur between the predictions and the demonstrated flight characteristics, and the improved values can only be obtained from the analysis of the flight data.

The wind-tunnel testing provided predictions of the stability and control derivatives.¹⁶ Estimates of the uncertainty in the predictions were also formulated. These uncertainties, called variations, are based on evaluation of previous correlations between wind-tunnel- and flight-determined coefficients for similar aircraft.¹⁷ These uncertainties were determined by a consensus of aerodynamicists and were based on their evaluations of past correlations with results from applicable configurations. These uncertainties are felt to be representative of the span of the uncertainty of pre-flight predictions.

To support the determination of the stability and control derivatives, the Space Shuttle carried the Aerodynamic Coefficient Instrumentation Package (ACIP) data collection system aloft, and maneuvers were performed during reentry for determination of these derivatives.¹⁵ The Space Shuttle was limited by not having acceptable flow-angle measurements, that is, angles of attack and sideslip (α and β), available above Mach 3. The flow angles determined from the inertial measurement unit (IMU) and the Best Estimated Trajectory (BET)¹⁵ were only available at 1 sample/sec, too low for dynamic analysis.

The parameter estimation problem (the determination of the stability and control derivatives from flight) can be defined quite simply in general terms. The system under investigation is assumed to be modeled by a set of dynamic equations containing unknown parameters. To determine the values of the unknown parameters, the system is excited by a suitable input, and the input and actual system response are measured. Values of the unknown parameters are then inferred based on the requirement that the computed model response to the given input match the actual, measured system response. When formulated in this manner, the unknown parameters can be identified easily by many methods. In the wind tunnel, the forces and moments are measured directly. In flight, only the response can be measured, and the forces and moments are derived from these responses.

The primary method of obtaining the stability and control derivatives from flight data uses the maximum-likelihood estimation method.¹⁸ This method also provides an estimate of uncertainty of each value. Space Shuttle stability and control derivatives were obtained with this method. All Space Shuttle flights to date have been analyzed with this maximum-likelihood estimator. The results of the analysis are used to support envelope expansion and to expand the fore and aft center-of-gravity limits for future payloads.

Figure 2 shows a longitudinal maneuver from the second Space Shuttle flight, STS-2, at a dynamic pressure of 17 lb/ft² and Mach 23. The figure shows time histories of the control inputs. These inputs include the up- and down-jets, body flap (BF), and elevator (symmetric elevon) deflection (δ_e). The figure also shows some of the dynamic responses of the vehicle, which are normal acceleration (a_n), pitch angle (θ), pitch rate (q), and angle of attack (α). The solid lines show the measured vehicle response, and the dotted lines show the maximum-likelihood-estimated model response.

One difficulty encountered with the Space Shuttle data was the relatively small amplitude of the maneuvers. The input must be large enough to sufficiently excite the system. For example on the first flight of the Space Shuttle, STS-1, most of the longitudinal maneuvers were very small incidental motions and frequently were about two orders of magnitude smaller than the maneuvers typical for most vehicles. The accuracy and scatter of the derivatives obtained from such small maneuvers were worse than would be expected from larger intentional maneuvers but were sufficient to establish some trends. A major issue in the analysis of the longitudinal maneuvers centered around the uncertainty in the center-of-pressure (CP) location, which is discussed in the Center-of-Pressure Location subsection. Even the maneuvers on later flights, designed for derivative determination, were small. The lateral-directional maneuvers were also quite small.

Figure 3 shows the coefficients of rolling and yawing moments due to angle of sideslip (C_{l_β} and C_{n_β}).¹⁹ This figure shows the predicted values with the expected variation and the flight-derived values with the estimated uncertainty. The flight C_{l_β} is less negative than predicted above Mach 10 and more negative below Mach 10. The flight C_{n_β} values oscillate around the prediction and stay within the variation, except near Mach 9.

Figure 4 shows the coefficients of rolling and yawing moments due to aileron (differential elevon) deflection ($C_{l_{\delta_a}}$ and $C_{n_{\delta_a}}$). The flight $C_{l_{\delta_a}}$ estimates were smaller than predicted between Mach 1 and 2 and slightly larger between Mach 14 and 22. The aileron derivatives for the third Space Shuttle flight, STS-3,

were somewhat larger in magnitude than for STS-1 and 2, probably because of the difference in average elevon deflection. The predictions had similar differences. Different surface schedules were used for the later flights. The flight $C_{n_{\delta_a}}$ estimates matched the predictions quite well below Mach 12 and were somewhat more negative between Mach 14 and 22.

The reason for the differences between predicted and flight values for these four key derivatives is unknown. The differences are attributed to tunnel noise, scale and real gas effects, and limited numbers of aerodynamic wind-tunnel tests above Mach 10.

Center-of-Pressure Location

The STS-1 showed that significantly more body-flap deflection was required to trim the vehicle hypersonically at an α of 40° than was predicted (Fig. 5).²⁰ During entry, the Space Shuttle is preprogrammed to fly at a given angle of attack for each Mach number. The angle of attack is maintained by setting the elevon at a position scheduled by angle of attack and Mach number. Then, the body flap is deflected to maintain the angle of attack. To maintain 40° angle of attack hypersonically on STS-1, the body flap was deflected to 16° instead of the predicted 7°. Because 9° more body-flap deflection than predicted was required, the body flap experienced more heating than predicted. The misprediction also resulted in the body flap being deflected to within 5° of its maximum deflection to trim the vehicle. In addition, more deflection of the body flap creates more drag, and this increased drag reduces the cross-range capability.

To examine this misprediction of body-flap trim position, the location of the CP was investigated. Figure 6 shows a comparison between flight and predicted locations of the CP plotted as a function of Mach number for STS-2.²¹ The variations for the prediction are also shown. The flight data were well outside of the predicted variations. Above Mach 16, the misprediction is about 0.8 percent of the body length, or 10 in. The error must be due to a misprediction of pitching moment, a misprediction of normal force, or an error in the location of the flight center of gravity. Error in the flight center-of-gravity position is less than 1 in. Also, the normal force predictions and flight values agreed fairly well; therefore, almost all of this 10-in. error was caused by a misprediction in the pitching moment. For the Space Shuttle, pitching moment is a function of coefficients of pitching moment due to angle of attack (C_{m_α}), pitching moment due to elevator deflection ($C_{m_{\delta_e}}$), pitching moment due to body flap deflection ($C_{m_{BF}}$), and pitching moment bias (C_{m_0}) at a given Mach number and angle of attack.

Figure 7 shows the flight-derived estimates of C_{m_α} , $C_{m_{\delta_e}}$, and $C_{m_{BF}}$ from the first three Space Shuttle

flights. Above Mach 16, the predictions and flight estimates agree well for these three derivatives. Thus, the error in body-flap deflection required for trim is attributable to C_{m_0} . The error in C_{m_0} that would account for the discrepancy shown in Fig. 6 would be about 0.03 nose up. An error in C_{m_0} up to about 0.020 to 0.025 can be attributed to the real gas effects and Mach number effects, neither of which were completely simulated in wind tunnels.^{22,23}

Between Mach 16 and 8, the CP-position misprediction went from 0.8 percent to less than 0.1 percent (Fig. 6). Real gas effects become less important as the Mach number decreases. Some of the error in CP-location prediction between Mach 16 and 8 may be attributed to the misprediction in boundary-layer transition. Preflight predictions indicated that boundary-layer transition would start to occur at Mach 16, but the flight data indicated that it transitions quickly at about Mach 8. Refer to the Boundary-Layer Transition sub-subsection for a more detailed discussion.

Reaction Control System Jet Interaction

Space Shuttle trajectory during reentry and, therefore, its heating profile are controlled through a series of energy-management bank reversals. The vehicle is controlled by conventional aerodynamic surfaces and reaction control system (RCS) jets. The first bank reversal on STS-1 resulted in a significantly larger response than predicted.²⁴

Figure 8 shows this flight maneuver at Mach 24 and compares it with the predicted maneuver. The flight maneuver resulted in angle of sideslip peaks twice the size of those predicted and in somewhat higher roll rates than predicted. Angle-of-sideslip excursions this large move an area of high heating off the reinforced carbon-carbon (RCC) noscap. The motion is also much more poorly damped than predicted. Comparing the predicted maneuver with the actual maneuver shows that the flight stability and control derivatives were significantly different from the predictions. These stability and control flight maneuvers were analyzed with the maximum-likelihood method. The resulting flight-determined estimates were used to significantly modify the flight simulator.

Simulation studies resulted in modifying the control inputs for the bank-reversal maneuver on STS-2, as shown in Fig. 9. Nearly identical maneuvers were flown on all subsequent Space Shuttle flights. The primary problem with this and other maneuvers at high altitude was obvious from the flight-determined rolling moment due to yaw jet (L_{YJ}). Figure 10(a) shows flight-determined and predicted L_{YJ} as a function of Mach number.¹⁹ The variations discussed in the Stability and Control Derivatives subsection are also evident on this figure. At the highest Mach numbers, the

value of the flight-determined L_{YJ} was outside these variations.

To understand the difference between flight and prediction, a brief description of how the predictions were made is necessary. More complete descriptions are given in Refs. 25 and 26. The forces and moments are broken down into three basic components: pure thrust, jet impingement on the Space Shuttle body, and jet interaction with the flow around the Space Shuttle. The jet-interaction term is the one of interest here, and the remainder of this discussion will concentrate on jet-interaction effects. The wind-tunnel tests were conducted for Mach numbers between 2.5 and 10. Since the wind-tunnel tests were limited to Mach numbers below 10 and dynamic pressures above 75 lb/ft², the predictions for higher altitudes and Mach numbers were obtained by varying momentum and mass-flow ratios to include those values applicable for the higher altitudes.

Figure 10(b) shows the comparison between the flight-determined and predicted jet-interaction terms. This figure shows that the flight rolling moment due to RCS jet interaction, determined with maximum-likelihood estimation, was smaller than predicted, particularly above Mach 15 at an altitude greater than 200,000 ft. The explanation for this high-altitude, jet simulation error lies in the description of the flow field surrounding the side-jet exhaust.²⁵ At high altitudes, the vehicle angle of attack is approximately 40°, which causes flow separation on the upper surface of the wing. When the RCS side jets are fired, the exhaust enters this separated flow region and pressurizes the volume defined by the wing upper surfaces and the flow-separation wake boundaries.

The aerodynamic flow field for this high-altitude flight environment cannot be properly simulated in the wind tunnel. For example, at the first bank maneuver (Fig. 8) at Mach 24, the flight dynamic pressure is 14 lb/ft². In these conditions, the wake boundary is much more easily deflected on the flight vehicle than on the wind-tunnel model. This difference in high-altitude pressure levels strongly influences the differences observed between flight and predicted side-jet rolling moment jet interaction. The phenomena are described more completely in Ref. 25.

These results show the limitations of the wind-tunnel database in predicting high-altitude jet effects. The vehicle wake-flow parameters, such as ambient pressure, cannot be duplicated in the tunnel.²⁵ Reference 26 presents the analysis of the limited amount of wing pressure flight data. The resulting trends for this analysis were similar to those discussed here for the maximum-likelihood results. Flight-derived forces and moments due to up-and-down-firing jets (used

primarily for pitch and roll commands at low dynamic pressure) have been discussed.^{19,25} The up-and-down-firing jets exhaust into the wakes generated by the fuselage and wing. The result is similar to that encountered with the side jets exhausting into the wake from the wing; the moments are overpredicted. Rolling moment of the roll jets and the pitching moment of the pitch jets in flight are smaller than predicted (Fig. 11). The correlation of these jet interaction terms has the same limitations as those discussed for rolling moment due to yaw jet.²⁵

Space Shuttle Heating

Heating is discussed in three sections: windward, leeward, and leading edge. The topic is discussed thusly because different physical phenomena influence the heating in these three areas.

Windward-Side Heating

The Space Shuttle has two significant causes of windward heating. The first is the chemical state of the flow, either equilibrium or nonequilibrium. In nonequilibrium flow, surface catalysis becomes an important element in heating. The second influence is the state of the boundary layer, either laminar or turbulent.

Catalytic Effects

The design of the TPS of the Space Shuttle orbiter was based on predicted aerothermodynamic environments which were generated assuming that the orbiter flow field was everywhere in chemical equilibrium.¹⁴ Detailed preflight calculations indicated, however, that significant chemical nonequilibrium would persist over the majority of that portion of orbiter entry when significant aerodynamic heat transfer occurs. The parameter which most significantly influences the level of surface heat transfer in such a flow field is the catalytic efficiency of the TPS surface with respect to the recombination of dissociated oxygen atoms. The catalytic efficiency of the reaction-cured glass (RCG) coating of the orbiter TPS tiles was thought to be relatively low, based on arc-tunnel experiments. Therefore, flight heating rates were expected to be lower than equilibrium chemistry predictions as a result of the combination of nonequilibrium chemistry and a non-fully-catalytic TPS surface. Indeed, surface temperatures were lower than the conservative predictions on the early flights.²⁷

In light of the great interest in noncatalytic surface effects, an experiment was conducted on STS-2 through -5 to study catalytic.²⁷ Thermal data for these especially modified tiles were collected on flights STS-2, -3, and -5. Selected centerline tiles with previously installed instrumentation were painted or overcoated

with highly catalytic material. The experiment was to demonstrate the noncatalytic nature of the baseline tiles by comparison with the characteristics of the more catalytic modified tiles. The flight data showed that the surface temperatures of the catalytically coated tiles (shown normalized) were substantially greater than those of the baseline tiles (Fig. 12); therefore, the surface catalytic efficiency of the baseline tiles is low.

An unexpected effect occurred during the entries that serendipitously provided further information into the catalytic and noncatalytic natures of orbiter windward-surface heat transfer.²⁸ This unplanned experiment manifested itself in significant instantaneous changes or jumps in measured TPS surface temperatures (Fig. 13) at affected locations. These jumps were apparently the result of anomalous deposition of metallic oxides on portions of the lower surface TPS because of oxidation of upstream acoustic sensor covers. These temperature jumps provided evidence of a sudden change in catalytic.

Comparing the levels of heat transfer between STS-2 and -3 for these locations showed an approximately 18 percent greater heating rate level below altitudes of about 238,000 ft on the later flight (Fig. 14). A mission-to-mission progressive contamination of the TPS surface was a contributing factor to this greater heating rate. This conclusion was bolstered by the good correlation between the postcontamination data from STS-2 (round symbols) and the data from STS-3 (square symbols) before additional contamination occurred (Fig. 15).

As the flight program progressed, changes in the windward surface from flight to flight became apparent.²⁷ The surface temperature was increased at the same flight condition compared with previous flights. This change led to the conclusion that the total emittance of the RCG coating decreased with the number of flights and surface catalytic efficiency of the coating increased or surface temperature increased with number of flights. The flight-to-flight changes in surface temperature can be seen in Fig. 12.

Surface contamination has been proposed as a possible cause of these changes. The general surface contamination comes from a variety of sources. These sources include impingement of burning solid rocket fuel and deposition of sea salt spray while on the pad. In addition, local contamination comes from the oxidation during entry of upstream metal acoustic sensor covers.

When the aerothermal design of the Space Shuttle first started, heating predictions were heavily based on wind-tunnel data, with modest computational modeling of catalytic.¹⁴ After the first five flights, heating predictions using computational models of the

nonequilibrium chemistry were in use.²⁷ The thermal response predictions made with these models, including ground-test data, design trajectory, and reacting boundary-layer computation, agreed well in general with the flight data (Fig. 16).

Nonequilibrium calculation techniques were used to predict heat fluxes to the windward side of the Space Shuttle orbiter.²⁹ The techniques were the axisymmetric viscous-shock-layer method, three-dimensional reacting Euler equations solutions coupled with axisymmetric analog boundary-layer method, and nonequilibrium three-dimensional viscous-shock-layer method. These calculation methods succeeded in predicting heating trends but did not predict the measurements uniformly over the entire windward centerline for all flight conditions. That is, nonequilibrium methodologies could predict the heat flux for high-altitude reentry, but some improvements were still required. In particular, the key issue was the modeling of catalytic efficiency.

At the current time, the models in use are capable of good agreement with the flight data as is shown in Fig. 17.³⁰⁻³² The addition of a recent correlation for oxygen surface recombination gave better overall agreement with the flight data than the extrapolation of ground-based experimental recombination data. Predicted centerline and windward-surface heat transfer were in good agreement with the flight data, and the predicted trends in heating rates away from the windward symmetry plane appear correct. Future application of the current code for three-dimensional vehicle analyses appears promising based on such verification.

This progress in modeling is the result of obtaining flight data from which to infer the catalytic efficiency of the tiles and increases in computational capability for model evaluation. This success in modeling the catalytic of Space Shuttle tiles using flight data indicates that obtaining flight data for other materials should result in good modeling of their catalytic.

In addition, the flight data also made it clear that the catalytic of a reusable vehicle should not be assumed to remain constant. Rather, catalytic may be changed by the flight process. Contamination (the melted acoustic covers and the launch plume impingement), ground handling (the sea spray from the launch pad environment), and other factors all may change the properties of the surface.

Boundary-Layer Transition

Knowing the time and position of the boundary-layer transition is fundamental to determining the heating on the windward side of the Space Shuttle. Boundary-layer transition strongly contributes to the heat load of the vehicle and the instantaneous heating rates. These

two factors are important in determining the thermal protection requirements of the vehicle.

A major element in boundary-layer transition is the roughness of the surface, such as the TPS tiles with which the windward surface is protected. To assess the effect of tiling patterns for these TPS tiles, a variety of grooves simulating tile gaps on flat plates were tested in the wind tunnel. Results showed that long grooves or gaps parallel to the streamlines produced more heating in the gaps. Grooves parallel to the surface streamlines produced strong boundary-layer-tripping disturbances whereas grooves perpendicular to the streamlines produced much weaker interactions.³³ From these results, the diagonal tiling pattern was established (Fig. 18).

In the original design, the tiled surface was assumed to be smooth, but actual fabrication revealed that the surface would be much rougher than planned.³⁴ The tiles were paved with nominal gaps of 0.045 in. and had rounded edges. In addition, the edges of some tiles were irregular because of manufacturing techniques. Thus, the surface was quite rough aerodynamically.³³ In fact, the lower surface with its steps, gaps, and tile irregularities is an incredibly complex surface in terms of roughness definition. Measurements of a number of areas that appeared to be typically rough (Fig. 19) confirm this complexity. The profilometer is able to resolve 0.001 in. surface displacements.

The original ground testing, assuming smoother tiles, was repeated for the rougher actual tiles. These tests prompted the development of a more refined aerothermodynamic database with improved prediction technologies. These tests influenced the layout and roughness criteria for tile installation.

Wind-tunnel tests were performed to examine boundary-layer transition using a 0.04-scale model with spherical roughnesses and simulated tiles. In the wind tunnel, the effects of the surface conditions dominated the upstream region, and the effects of tunnel noise dominated the transition process in the downstream region. These effects suggest that transition predictions would be conservative in the downstream region and reasonably reliable in the upstream region.³⁴

Original predictions indicated that transition would start at the aft end of the vehicle at about 900 sec and slowly move forward (Fig. 20). In flight, transition started much later than predicted and flashed to the nose almost instantaneously, as is also apparent in Fig. 20.

Figure 21 shows this rapid transition more graphically with transition maps for STS-2 through STS-5.³⁵ The transition contours for the left side of the Space Shuttle (the instrumented side) are mapped onto the

Space Shuttle planform for four flight conditions. In Fig. 21(a), the transition front can be observed to flash forward instantaneously (i.e., between time $(\pm t) = 76,297$ and $76,298$ sec) from the aft of the vehicle toward the nose. Figure 21 shows that the transition front flashed forward in 4 sec or less on STS-2 through STS-5. The complexity of the transition contours and the abrupt manner in which they were moved strongly indicate that the inflight transition process is dominated by the effects of discrete surface roughness.

On STS-3 (Fig. 21(b)) the transition occurred at about the same flight conditions as on STS-2 (Fig. 21(a)). However, the STS-4 transition (Fig. 21(c)) occurred at a higher Mach number, higher angle of attack, and lower Reynolds number. On STS-5 (Fig. 21(d)), the transition occurred at intermediate values of angle of attack and Mach number and at a substantially lower Reynolds number than on STS-2 and STS-3. These data are not conclusive, but the trend indicates that in-flight transition, in addition to being a function of Mach number, may also be a function of angle of attack; that is, at higher angles of attack the flow transitions at a higher Mach number. Reference 34 states that between angles of attack of 25° and 40° , the wind-tunnel data base has indicated very little effect of angle of attack alone on transition.

Reference 33 notes that on STS-1, the flow transitioned to turbulent at one wing station for 7 sec and then returned to laminar flow for 26 sec before it finally transitioned to turbulent flow and remained turbulent for the remainder of this flight. In this instance, the angle of attack dipped during the period of relaminarization of the flow. Angle of attack, therefore, may have contributed to this relaminarization. This result, with the potential angle-of-attack effect noted previously, may indicate that the flight data show that increased angle of attack may cause earlier boundary-layer transition in flight.

The transition from laminar to turbulent flow at the aft end of the vehicle occurred later in the entry than expected and produced lower temperatures and total heat load.³⁶ Figure 22 shows the predicted and flight values of lower-surface temperatures at the 70-percent location. The delay in transition can be clearly seen in the delayed increase in temperature.

Based on postflight analysis, the predictions could apparently have been improved by removing the original, smooth-surface data from the correlation parameter because these data were very sensitive to free-stream noise. However, even the rough-surface data seemed to be very sensitive to tunnel noise.

The good agreement between the predicted and measured transition times in such regions as the 10- to 20-percent centerline suggested that the simulation and

correlation of transition in certain regions was very good.³³ The regions for which the agreement was good had the transition process dominated by surface roughness and shock-layer disturbances at both wind-tunnel and flight conditions. The two phenomena probably dominated because of the relatively thin boundary layer and highly curved bow shock near the forward part of the orbiter. From the above rationale, the conclusion was reached that the wind-tunnel data generated with effective roughnesses provided good predictions of flight conditions for the forebody. Differences between predictions and flight values for the aft region were attributed to tunnel noise.

Leeward-Side Heating

Leeward-side heating is a highly complex three-dimensional process dominated by separated and reattaching flows as well as vortex scrubbing and impingement. Areas heated by this process include the top and sides of the fuselage and the orbital maneuvering system (OMS) pods. Figure 23 shows the different types of fuselage side heating caused by lee-side vortex flows.

Top Centerline Heating

Heating on top of the orbiter separated-flow-dominated fuselage is quite complex, and the upper fuselage thermal environment is generally characterized in terms of heating to the leeward centerline. An empirical technique for predicting top centerline heating on the orbiter was developed.³⁷ This technique consisted of a modified turbulent swept-cylinder correlation using an effective local sweep angle that was measured directly from oil-flow patterns from wind-tunnel tests. These wind-tunnel sweep angles were then extrapolated to account for conditions at flight Reynolds numbers and Mach numbers. Reference 37, using this approach, showed that the leeward centerline methodology is able to predict the diverse heating environment represented by the wind-tunnel data.

A relatively simple approach for extrapolating the leeward centerline heating equation and wind-tunnel sweep angles to flight conditions was established. The first step was to establish a procedure for extrapolating wind-tunnel sweep angles to equivalent flight Reynolds number values. The next step was to define a criterion that related the flight environment at each trajectory point to the proper set of wind-tunnel test conditions. The final step was to develop a method of correcting for the effects of the differential between flight Mach numbers and the wind-tunnel Mach numbers from which the flight sweep-angle distribution was extrapolated.

The predictions and flight data compared well for Mach numbers below 15, but the predictions were higher than the flight data for Mach numbers above 15 (Fig. 24).³⁸⁻⁴¹ One hypothesis for this difference

is that laminar flow existed on the lee side above Mach 15, whereas the prediction methodology assumed turbulent flow. This hypothesis is supported by Ref. 38, which discusses the discovery of a distinct transition of the lee side flow field from laminar to turbulent at about Mach 15. This sudden transition from laminar to turbulent is shown at the bank reversal at Mach 15 in Fig. 24.

Side-Fuselage Heating

An empirical method for predicting side-fuselage impingement heating was also developed based on analysis of oil-flow patterns and phase-change paint and thermocouple (T/C) heating measurements. The same type of turbulent heating equation that was used for the top centerline model is used in this method. The surface oil-flow patterns indicate angle of attack of the flow on the side fuselage or a sweep angle as described in the Top Centerline Heating subsection.

The source of the impinging flow was assumed to be the shear layer which originates along a separation line on the upper surface of the strake. Figure 25 shows the predicted location of the impingement line and the location of the side-fuselage instrumentation.

Limited flight data showed mostly good agreement with the predictions (Fig. 26). The isolated cases where the flight data shows much higher values, or *spikes*, have been attributed to embedded vortices generated by viscous interactions during the impingement process. These spikes were also seen in the wind-tunnel data. The embedded vortices are believed to be caused by boundary-layer cross-flow instabilities. In the wind-tunnel testing, a sequence of uniformly spaced streaks in phase-change paint above and originating from the impingement location on the side fuselage of the model was seen. Each streak is thought to represent a very thin line of vortex impingement which produces locally higher heating.

OMS Pod Heating

The OMS pod has been investigated extensively because the heating of the pod is a critical factor in the ability of the orbiter to fly reduced angles of attack relative to development flight test and current operational levels.⁴² Extending from the orbiter side makes the OMS pod extremely susceptible to flow impingement or vortex scrubbing and to damage from debris traversing along the fuselage (Figs. 1 and 23). In all leeward-side regions strongly influenced by vortex scrubbing, the wind-tunnel data underpredicted the flight test data.⁴² This scrubbing is reflected in Fig. 27, showing both predicted and flight temperatures for STS-2.

Vortex scrubbing is extremely sensitive to small variations in angle of attack, yaw, and Reynolds number.

In flight, the flow appeared to become attached at a higher angle of attack and at a lower Reynolds number than under wind-tunnel conditions. This sensitivity to angle of attack and flow attachment is particularly evident (Fig. 27) in the data collected in pull-up-push-over (POPU) maneuvers, which are characterized by large variations in angle of attack. The change in temperature during the POPU at Mach 20 is very obvious and it can also be seen that the methodology did not predict this sensitivity.³⁶ The methodology did not predict this sensitivity because the wind tunnel predicted that the impingement would occur near 30° rather than at 37° as seen in flight.

Wing Leading-Edge Heating

"Boundary-layer" heating and shock interaction are the two sources of heating of the wing leading edge.⁴³ For lack of a better term, we use *boundary-layer heating* here to mean the heating where there is no shock interaction. The instrumentation of the leading edge was designed to measure the effects of both types of heating.

Instrumentation (radiometers) was installed (Fig. 28) at stations 40-, 55-, 80-, and 98.6-percent semispan, and data were collected during the first five flights. The 40-percent semispan is on the glove, and the 98.6-percent semispan is at the wingtip. The 55-percent semispan is in the peak entry heating zone caused by shock interaction, and the 80-percent semispan is in the maximum entry airload zone. The Wing-Shock Interaction subsection discusses the 55-percent shock interaction.

Figure 29 shows the maximum heat rate of the leading edge, with the predicted values and flight radiometer data, and the estimated values from the radiometer data and the model.

Wing Boundary-Layer Heating

The wing leading edge of the Space Shuttle was aerothermodynamically modeled in a simplified form as a 45-deg swept cylinder with regions of higher sweep at the glove and the wing tip. Wind-tunnel data were used with this model to produce the predictions before flight. This method did not model the shock interaction at the 55-percent semispan location.

The predicted temperature at the 80-percent semispan (panel 16) matched the flight data extremely well (Fig. 30). The flight-estimated values based on the radiometer data were within 2 percent of the preflight prediction. This good match verified the usability of swept-cylinder methods outside the shock-interaction zone.

The heat rates in the glove (represented by the 40-percent semispan) and the wingtip (the 98.6-percent

semispan) were substantially overpredicted. On the other hand, this overprediction had been expected since the swept-cylinder approach is known to be conservative in regions of high sweep.

The onset of boundary-layer transition that was assumed in the prediction would have caused more heating at the wingtip. However, the actual transition behavior was quite different from that predicted, and this additional heating did not occur. Thus, the existing wingtip-analysis method was adequate for predicting flight heating and overpredicted with respect to the predicted heating because of transition.⁴³

Wing-Shock Interaction

In addition to the boundary-layer heating that heats the entire leading edge, bow- and leading-edge-shock interaction heats the leading edge locally.⁴³ Analysis of schlieren data, oil-flow patterns, and heat-transfer data from wind-tunnel tests indicated that the bow and leading-edge shock impinged with a resulting third shock and vortex/jet impinging on the wing. The main effects of this disturbance were expected to be increased shock-interaction heating at 55-percent semispan on the leading edge, earlier transition on the outboard portions of the wing lower surface, and increased vortex scrubbing on the outboard wing upper surface.

This shock impingement is difficult to scale from the wind tunnel to flight, so following- and double-shock techniques were used to scale wind-tunnel data to predicted flight conditions.⁴³ As mentioned in the Wing Leading-Edge Heating subsection, instrumentation was installed at 55-percent semispan (panel 9) to measure the heating because of the shock interaction.

The predicted temperature was 200 °F lower than that measured in flight during the period of peak heating (Fig. 31). This higher measured temperature is confirmed by the temperature distribution shown in Fig. 32.

On subsequent flights, the temperature in this region was consistently about 200 °F higher than the predicted values. This difference confirms the difficulty of scaling wing-shock interaction from the wind tunnel to flight.

Concluding Remarks

Correlation and validation of ground test and flight are used in a complimentary fashion to improve the results of both. The flight data provide benchmark data to improve interpretation and corrections to ground test results. These improved ground test techniques, coupled with other flight test data, allow improved

vehicles to be designed, built, and analyzed with reduced technical risk.

Many examples show that the predictions from ground-based data were conservative. Such results are expected as uncertainty should result in conservative predictions. The objective is to design the flight vehicle with adequate margins to reduce the risk to the vehicle. At the same time, these margins must be kept low enough that the flight vehicle is versatile, and its useful flight envelope can be expanded during flight test. Of course, much is learned in the validation of ground test with flight data even if the prediction agrees completely with flight. This agreement further reduces the margins required for future flight vehicles.

In some cases, however, even the conservative ground test predictions are exceeded. When this happens much more is learned, assuming that the vehicle survives, as we may become aware of new phenomena or of the increased importance of old phenomena. The Space Shuttle exceeded the conservative predictions and their associated uncertainties in four primary areas. These areas include the center-of-pressure location, reaction control system jet interaction with the flow over the vehicle, angle of attack at which the vortex impinged on the OMS pod, and wing leading-edge shock-interaction heating. None of these cases where the conservative predictions were exceeded by the flight values resulted in the loss of the vehicle. Survival of the vehicle is a tribute to the overall design philosophy, including ground test predictions, and to the designers of the Space Shuttle.

References

¹Ried, R.C., Jr., W.C. Rochelle, and J.D. Milhoan, *Radiative Heating to the Apollo Command Module: Engineering Prediction and Flight Measurement*, NASA TM X-58091, 1972.

²Sutton, Kenneth, "Air Radiation Revisited," in *Progress in Astronautics and Aeronautics: Thermal Design of Aeroassisted Orbital Transfer Vehicles*, vol. 96, H.F. Nelson, ed., 1985, pp. 419-441. (Also available as AIAA-84-1733, June 1984.)

³Wright, R.L. and E.V. Zoby, "Flight Boundary Layer Transition Measurements on a Slender Cone at Mach 20," AIAA 77-719, June 1977.

⁴*Review of the X-15 Program*, Weil, Joseph, comp., NASA TN D-1278, 1962.

⁵Becker, John V., "The X-15 Project," *Astronaut. & Aeronaut.*, Feb. 1964, pp. 52-61.

⁶Toll, Thomas A. and Jack Fischel, "The X-15 Project: Results and New Research," *Astronaut. & Aeronaut.*, Feb. 1964, pp. 20-28.

⁷Becker, John V., *The X-15 Program in Retrospect*, 3rd Eugen Sänger Memorial Lecture, Deutsch Gesellschaft für Luft und Raumfahrt, Dec. 1968.

⁸Williamson, W.E., Jr., "Hypersonic Flight Testing," AIAA 92-3989, July 1992.

⁹*Shuttle Performance: Lessons Learned*, NASA CP 2283, pts. 1 and 2, 1983.

¹⁰Meyer, Robert R., Robert E. Curry, and Gerald D. Budd, "Aerodynamic Flight Research Using the Pegasus Air-Launched Space Booster," AIAA 92-3990, July 1992.

¹¹*Space Shuttle Technical Conference*, NASA CP-2342, June 1983.

¹²Iliff, Kenneth W. and Mary F. Shafer, "A Comparison of Hypersonic Flight and Prediction Results," AIAA-93-0311, Jan. 1993.

¹³Young, James C., et al., "The Aerodynamic Challenges of the Design and Development of the Space Shuttle Orbiter," in *Space Shuttle Technical Conference*, NASA CP-2342, 1983, pp. 209-263.

¹⁴Ried, Robert C., "Orbiter Entry Aerothermodynamics, in *Space Shuttle Technical Conference*, NASA CP-2342, 1983, pp. 1051-1061.

¹⁵Throckmorton, David A., "Shuttle Entry Aerothermodynamic Flight Research: The Orbiter Experiments (OEX) Program," AIAA 92-3987, July 1992.

¹⁶*Aerodynamic Design Data Book Orbiter Vehicle STS-1*, SD72-5H-0060 revision M, Rockwell International, Nov. 1980.

¹⁷Young, James C. and Jimmy M. Underwood, "The Development of Aerodynamic Uncertainties for the Space Shuttle Orbiter," in *Shuttle Performance: Lessons Learned*, NASA CP-2283, pt. 2, 1983, pp. 1169-1185.

¹⁸Iliff, Kenneth W., Richard E. Maine, and Douglas R. Cooke, "Selected Stability and Control Derivatives From the First Space Shuttle Entry," AIAA 81-2451, Nov. 1981.

¹⁹Maine, R.E. and K.W. Iliff, "Selected Stability and Control Derivatives From the First Three Space Shuttle Entries," AIAA 82-1318, Aug. 1982.

²⁰Kirsten, Paul W., David F. Richardson, and Charles M. Wilson, "Predicted and Flight Test Results of the Performance, Stability and Control of the Space Shuttle From Reentry to Landing," in *Shuttle Performance: Lessons Learned*, NASA CP-2283, pt. 1, 1983, pp. 509-524.

²¹Romere, Paul O. and A. Miles Whitnah, "Space Shuttle Entry Longitudinal Aerodynamic Comparisons

Of Flights 1-4 With Preflight Predictions," in *Shuttle Performance: Lessons Learned*, NASA CP-2283, pt. 1, 1983, pp. 283-307.

²²Woods, W.C., J.P. Arrington, and H.H. Hamilton II, "A Review of Preflight Estimates of Real-Gas Effects on Space Shuttle Aerodynamic Characteristics," in *Shuttle Performance: Lessons Learned*, NASA CP-2283, pt. 1, 1983, pp. 309-346.

²³Griffith, B.J., J.R. Maus, and J.T. Best, "Explanation of the Hypersonic Longitudinal Stability Problem—Lessons Learned," in *Shuttle Performance: Lessons Learned*, NASA CP-2283, pt. 1, 1983, pp. 347-380.

²⁴Iliff, Kenneth W., *Aircraft Parameter Estimation AIAA Dryden Lecture in Research for 1987*, NASA TM-88281, 1987. (Also available as AIAA 87-0623, Jan. 1987.)

²⁵Stone, J.S., J.J. Baumbach, and B.B. Roberts, "Space Shuttle Orbiter Reaction Control Subsystem Flight Data Anomalies," in *Shuttle Performance: Lessons Learned*, NASA CP-2283, pt. 1, 1983, pp. 381-395.

²⁶Scallion, W.I., et al., "Space Shuttle Third Flight (STS-3) Entry RCS Analysis," AIAA 83-0116, Jan. 1983.

²⁷Stewart, David A., John V. Rakich, and Martin J. Lanfranco, "Catalytic Surface Effects on Space Shuttle Thermal Protection System During Earth Entry of Flights STS-2 through STS-5," in *Shuttle Performance: Lessons Learned*, NASA CP-2283, pt. 2, 1983, pp. 827-846.

²⁸Throckmorton, David A., E. Vincent Zoby, and H. Harris Hamilton II, "Orbiter Catalytic/Noncatalytic Heat Transfer as Evidenced by Heating to Contaminated Surfaces on STS-2 and STS-3," in *Shuttle Performance: Lessons Learned*, NASA CP-2283, pt. 2, 1983, pp. 847-864.

²⁹Scott, Carl D., "A Review of Nonequilibrium Effects and Surface Catalysis on Shuttle Heating," in *Shuttle Performance: Lessons Learned*, NASA CP-2283, pt. 2, 1983, pp. 865-889.

³⁰Thompson, R.A., "Comparison of Nonequilibrium Viscous-Shock-Layer Solutions with Shuttle Heating Measurements," *J. Thermophysics and Heat Transfer*, vol. 4, no. 2, Apr. 1990, pp. 162-169.

³¹Scott, Carl D., "Catalytic Recombination of Nitrogen and Oxygen in High-Temperature Reusable Surface Insulation," in *Progress in Astronautics and Aeronautics: Aerothermodynamics and Planetary Entry*, vol. 77, 1981, pp. 192-212. (Also available as AIAA 80-1477, July 1980.)

³²Zoby, E.V., R.N. Gupta, and A.L. Simmonds, "Temperature-Dependent Reaction Rate Expressions for Oxygen Recombination," in *Progress in Astronautics and Aeronautics: Thermal Design of Aeroassisted Orbital Transfer Vehicles*, vol. 96, H.F. Nelson, ed., 1985, pp. 445-465. (Also available as AIAA 84-0224, Jan. 1984.)

³³Harthun, M.H., C.B. Blumer, and B.A. Miller, "Orbiter Windward Surface Entry Heating: Post-Orbital Flight Test Program Update," in *Shuttle Performance: Lessons Learned*, NASA CP-2283, pt. 2, 1983, pp. 781-804.

³⁴Goodrich, Winston D., Stephen M. Derry, and John J. Bertin, "Shuttle Orbiter Boundary Layer Transition at Flight and Wind Tunnel Conditions," in *Shuttle Performance: Lessons Learned*, NASA CP-2283, pt. 2, 1983, pp. 753-779.

³⁵Hartung, L.C. and D.A. Throckmorton, "Computer Graphic Visualization of Orbiter Lower Surface Boundary-Layer Transition," *J. Spacecraft and Rockets*, vol. 24, no. 2, Mar.-Apr. 1987, pp. 109-114.

³⁶Hertzler, Elam K. and Paul W. Phillips, "Flight Test-Derived Heating Math Models for Critical Locations on the Orbiter During Reentry," in *Shuttle Performance: Lessons Learned*, NASA CP-2283, pt. 2, 1983, pp. 703-718.

³⁷Helms, Vernon T., III, "Leeward Centerline and Side Fuselage Entry Heating Predictions for the Space

Shuttle Orbiter," in *Shuttle Performance: Lessons Learned*, NASA CP-2283, pt. 2, 1983, pp. 913-947.

³⁸Throckmorton, D.A. and E.V. Zoby, "Orbiter Entry Leeward Heat-Transfer Data Analysis," *J. Spacecraft and Rockets*, vol. 20, no. 6, Nov.-Dec. 1983, pp. 524-530.

³⁹Herrera, B.J., *Results From a Convective Heat Transfer Rate Distribution Test on a 0.0175 Scale Model (22-0) of the Rockwell International Vehicle 4 Space Shuttle Configuration in the AEDC-VKF Tunnel B (OH49B)*, NASA CR-147626, 1976.

⁴⁰Helms, Vernon T., III, "An Empirical Method for Computing Leeward Centerline Heating on the Space Shuttle Orbiter," *J. Spacecraft & Rockets*, vol. 20, May-June 1983, pp. 225-231.

⁴¹Bertin, John J. and Winston D. Goodrich, "Effects of Surface Temperature and Reynolds Number on Leeward Shuttle Heating," *J. Spacecraft & Rockets*, vol. 13, no. 8, Aug. 1976, pp. 473-480.

⁴²Haney, J.W., "Orbiter Entry Heating Lessons Learned From Development Flight Test Program," in *Shuttle Performance: Lessons Learned*, NASA CP-2283, pt. 2, 1983, pp. 719-751.

⁴³Cunningham, John A. and Joseph W. Haney, Jr., "Space Shuttle Wing Leading Edge Heating Environment Prediction Derived From Development Flight Test," in *Shuttle Performance: Lessons Learned*, NASA CP-2283, pt. 2, 1983, pp. 1083-1109.

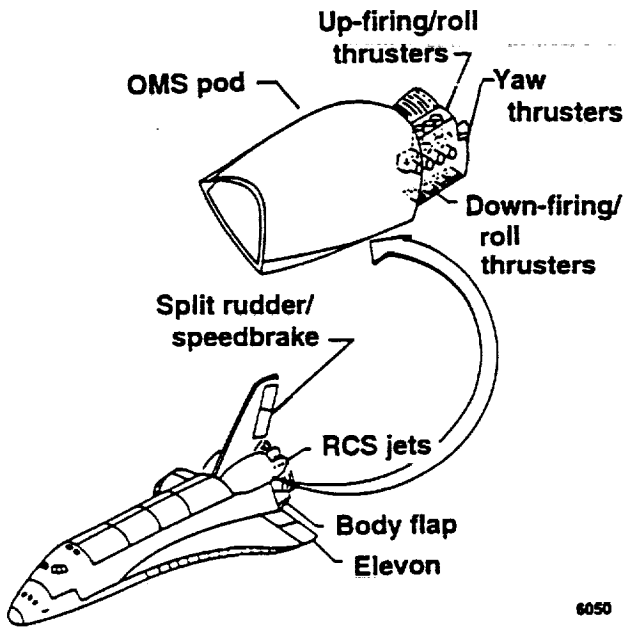


Fig. 1 Space Shuttle configuration.

6050

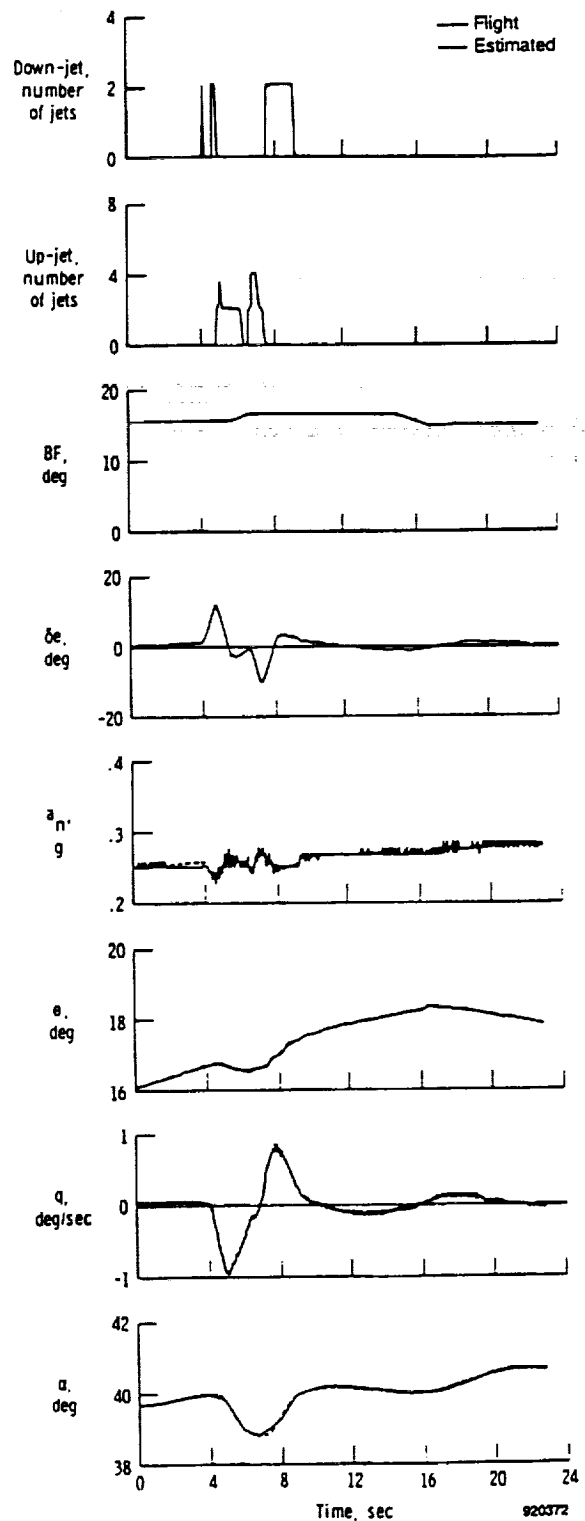


Fig. 2 Intentional longitudinal maneuver: STS-2 (from Ref. 19).

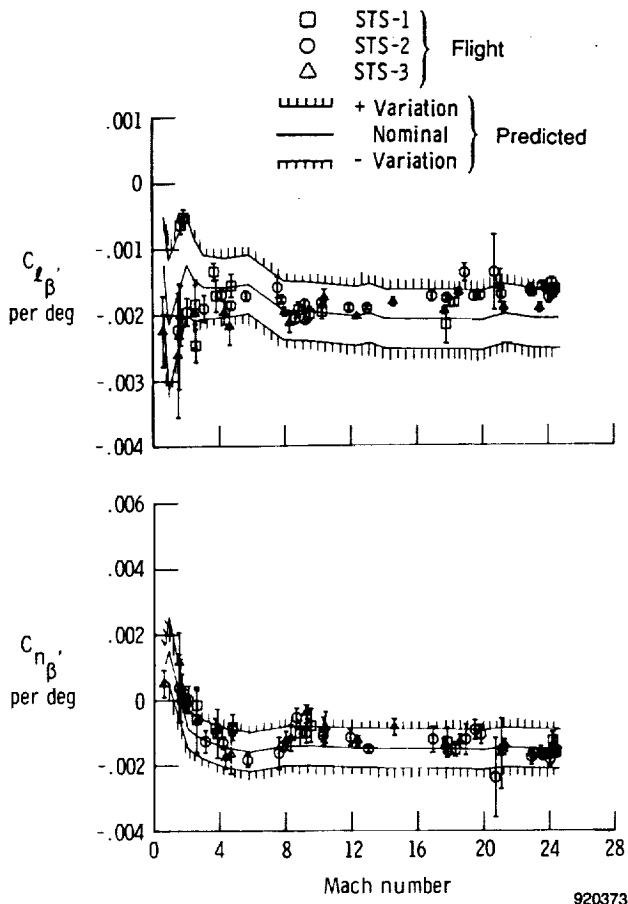


Fig. 3 Rolling and yawing moments due to sideslip (from Ref. 19).

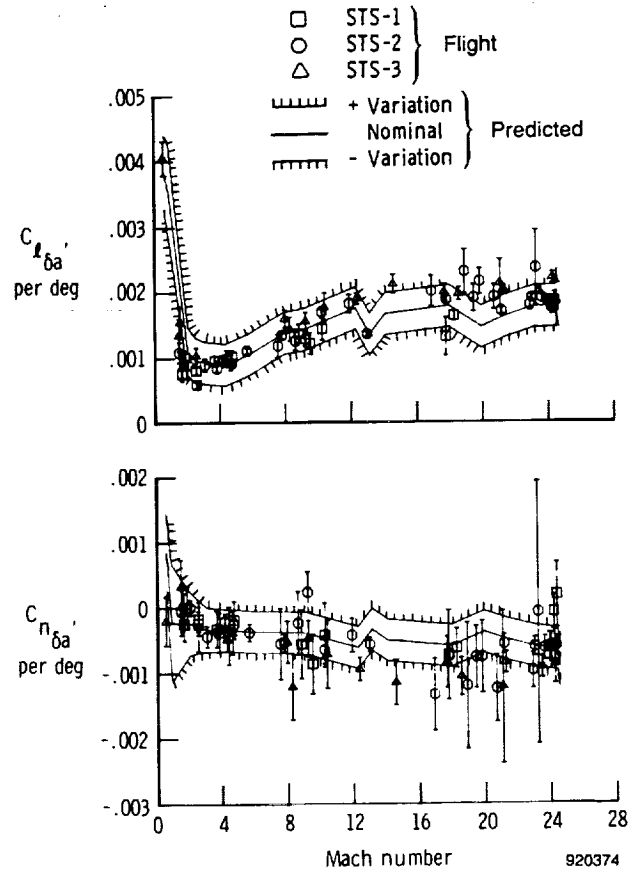


Fig. 4 Rolling and yawing moments due to aileron deflection (from Ref. 19).

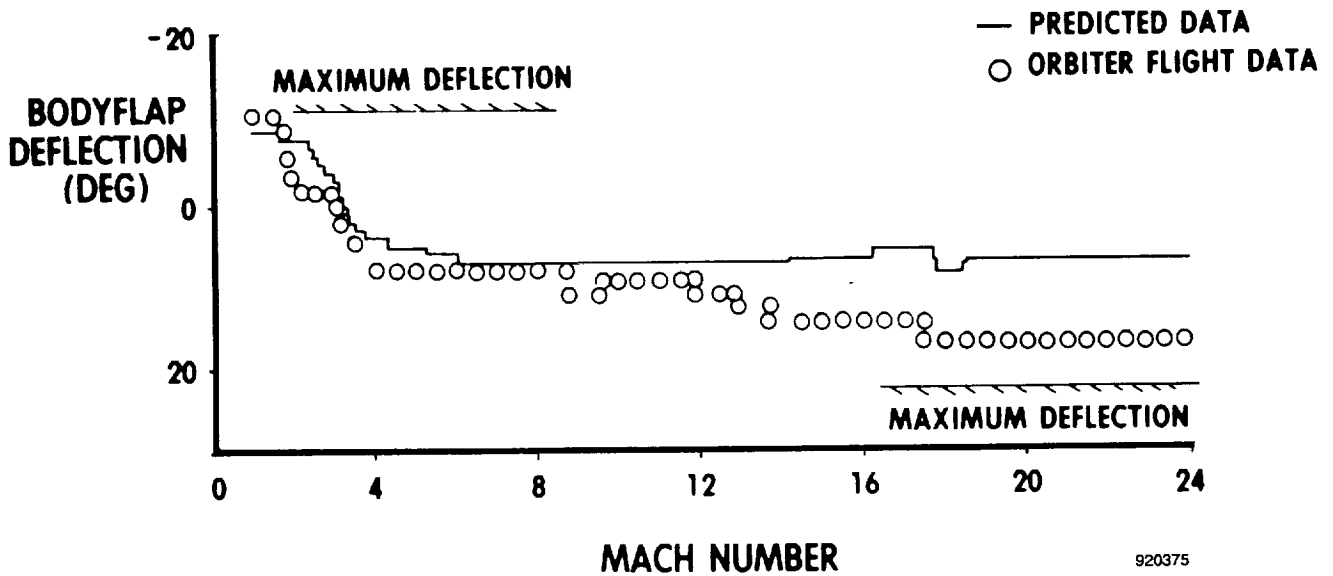


Fig. 5 Longitudinal trim characteristics from STS-1 (from Ref. 20).

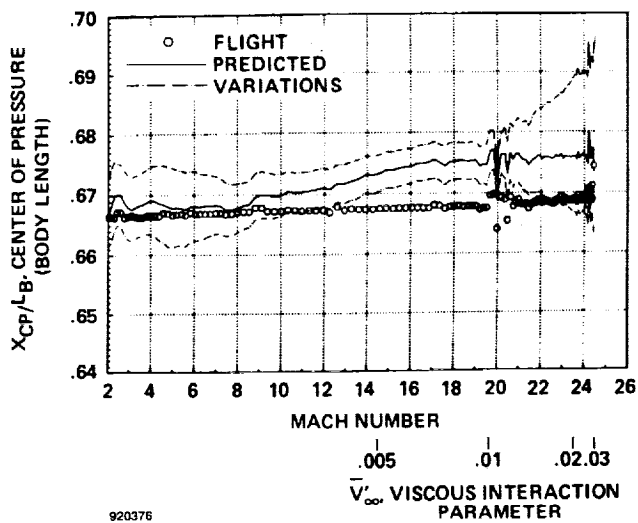


Fig. 6 The STS-2 longitudinal aerodynamic center-of-pressure location comparison (from Ref. 21).

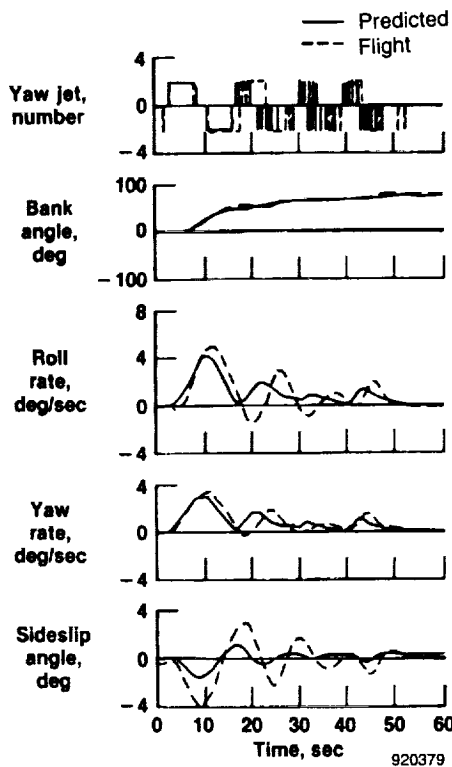


Fig. 8 Comparison of flight and predicted STS-1 maneuver at Mach 24 (from Ref. 24).

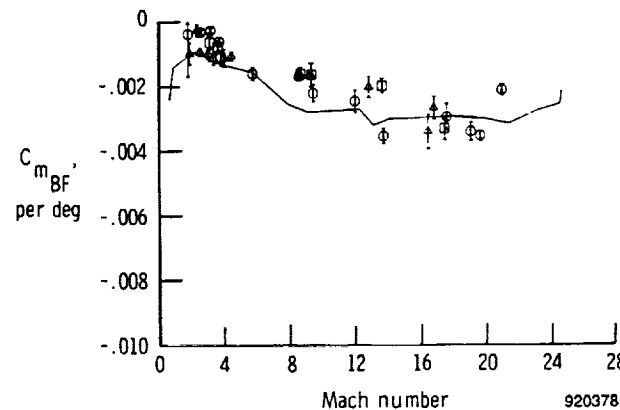
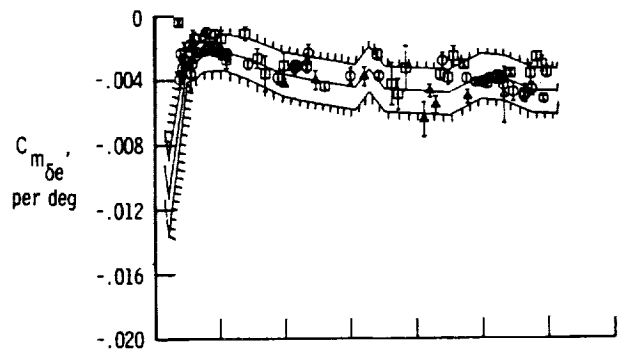
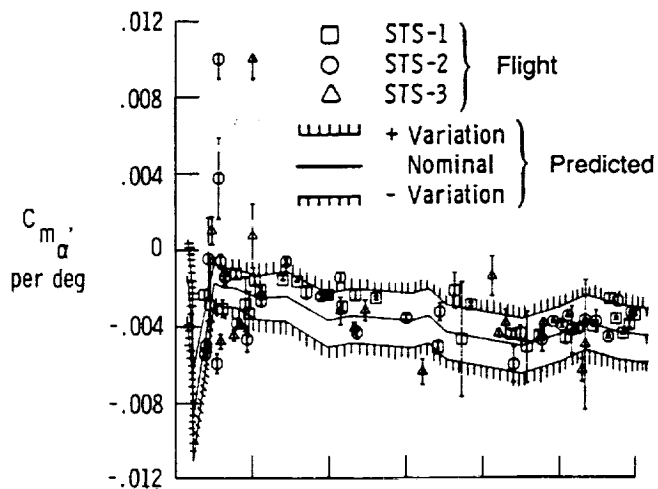


Fig. 7 The coefficients of pitching moment due to angle of attack, elevator deflection, and body flap deflection (from Ref. 19).

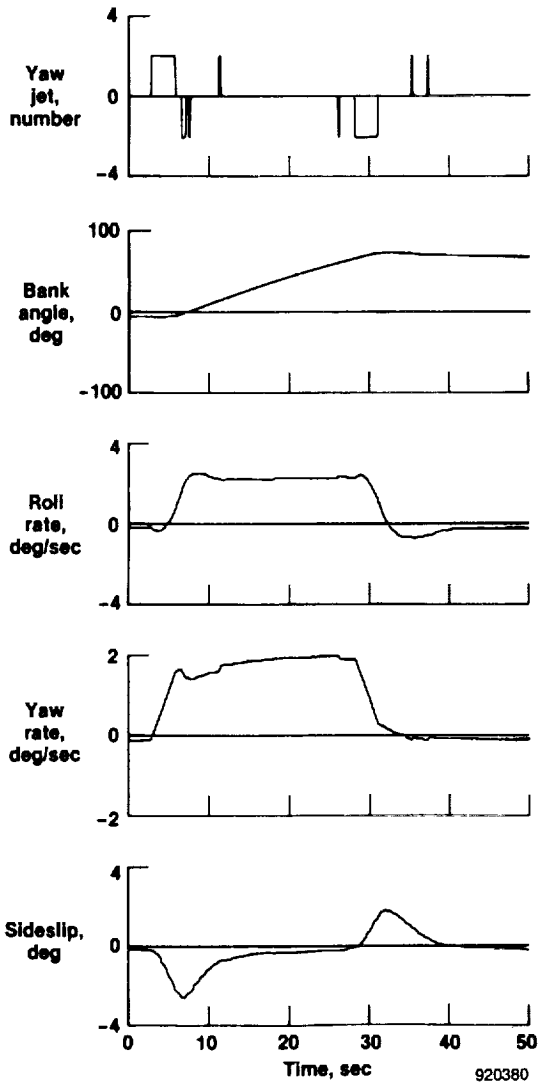


Fig. 9 Manual bank maneuver at Mach 24 from STS-2 (from Ref. 24).

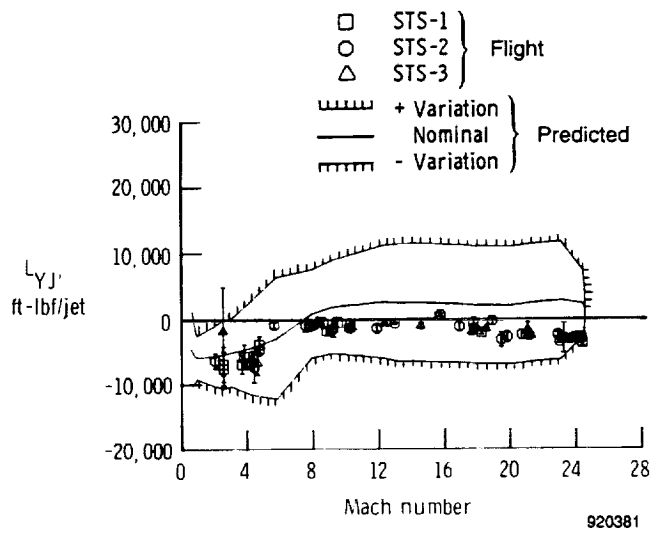


Fig. 10 The rolling moment due to yaw jet as a function of Mach number (adapted from Ref. 19).

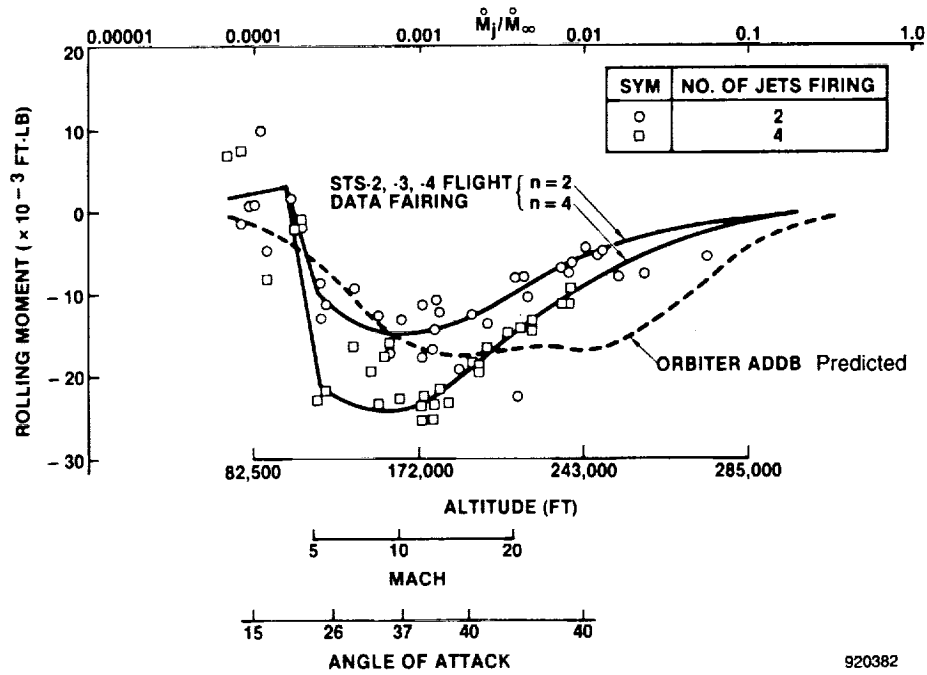


Fig. 11 Yaw jet rolling moment interaction (from Ref. 25).

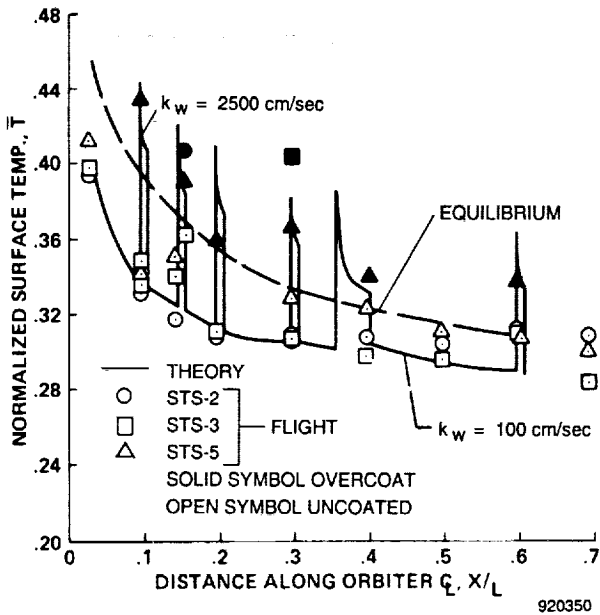


Fig. 12 Surface temperature distribution along mid-fuselage centerline (from Ref. 27).

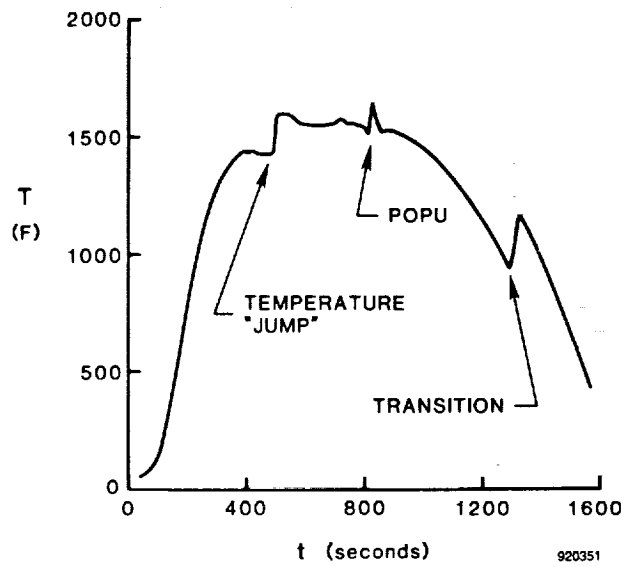


Fig. 13 The STS-2 temperature time history at $X/L = 0.194$ (from Ref. 28).

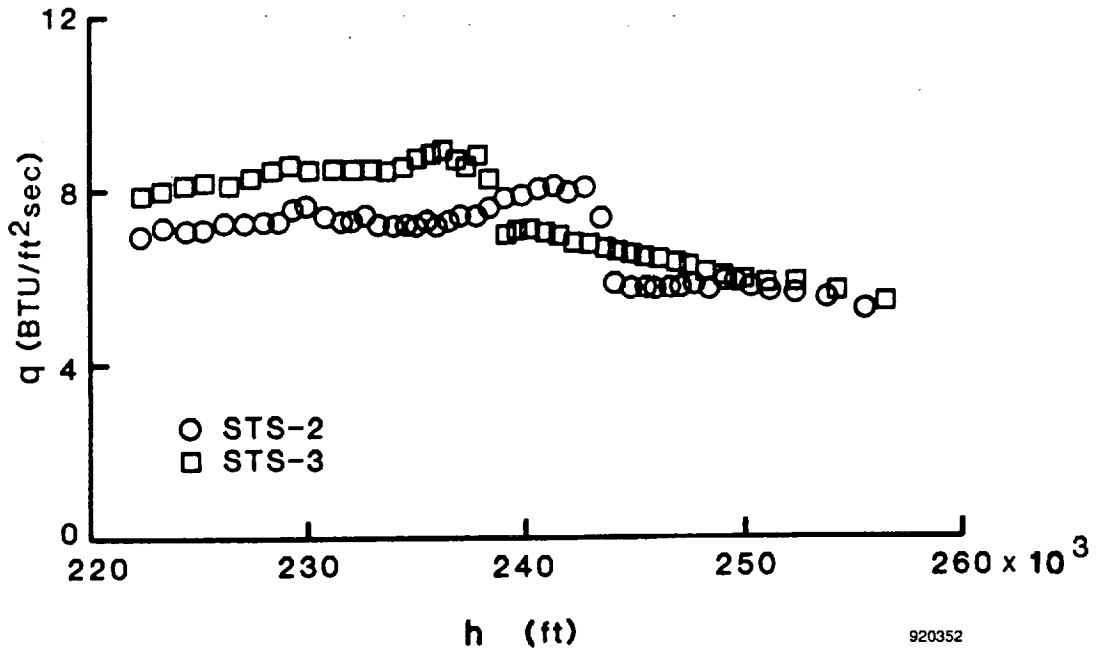


Fig. 14 Heat transfer to tile on flights STS-2 and STS-3 at $X/L = 0.194$ (from Ref. 28).

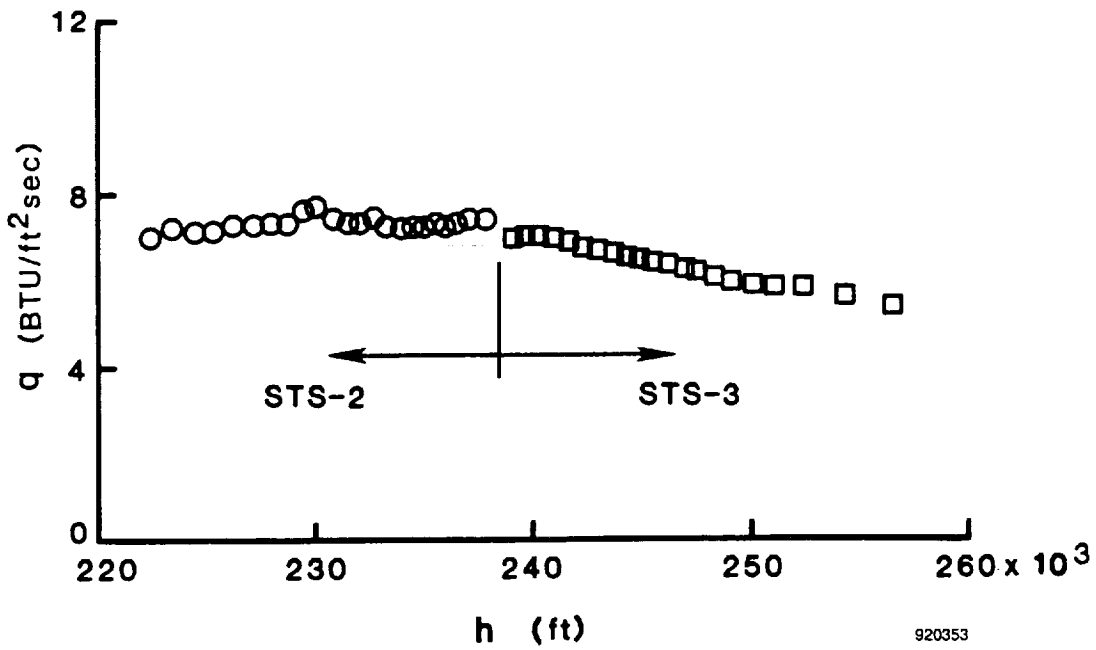


Fig. 15 Heat transfer to tile before and after contamination in flight at $X/L = 0.194$ (adapted from Ref. 28).

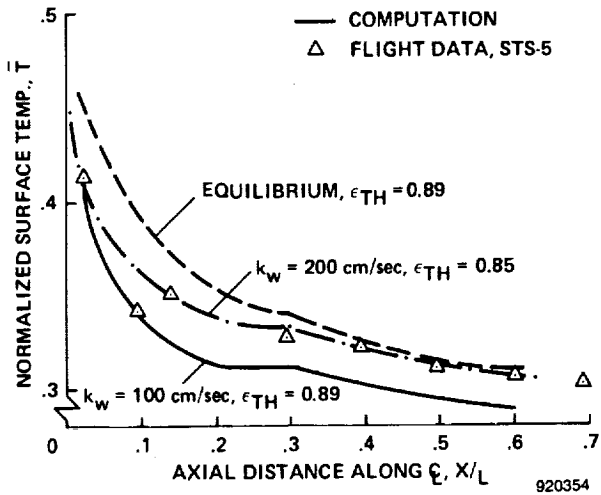


Fig. 16 Comparison of measured and predicted surface temperatures using postflight STS-5 reaction-cured glass surface properties at $M_\infty/\sqrt{R_\infty} = 0.0304$ for STS-2 (from Ref. 27).

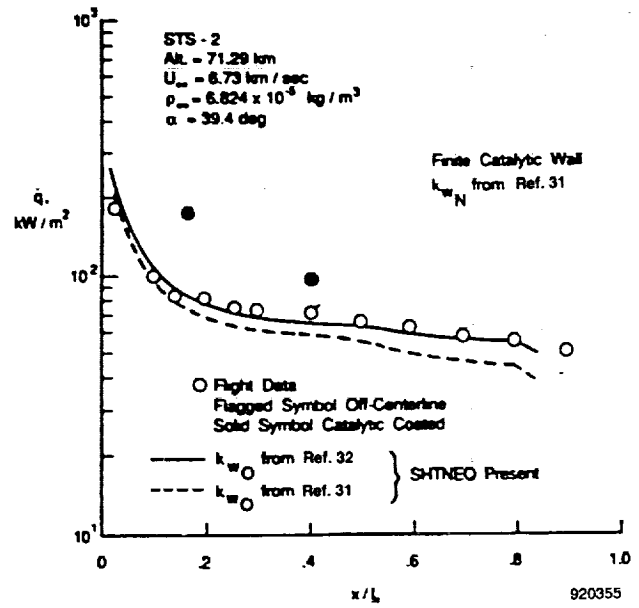


Fig. 17 Nonequilibrium heat-transfer prediction along the windward centerline at an altitude of 71 km (adapted from Ref. 30).

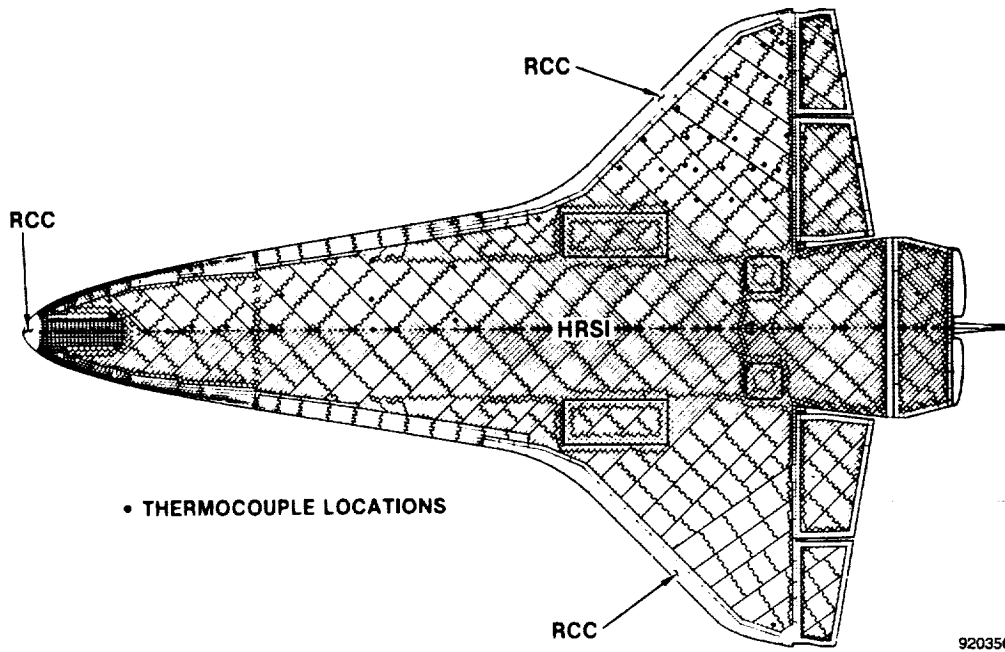


Fig. 18 Orbiter lower surface tile pattern and surface thermocouple layout (from Ref. 33). [Not to scale.]

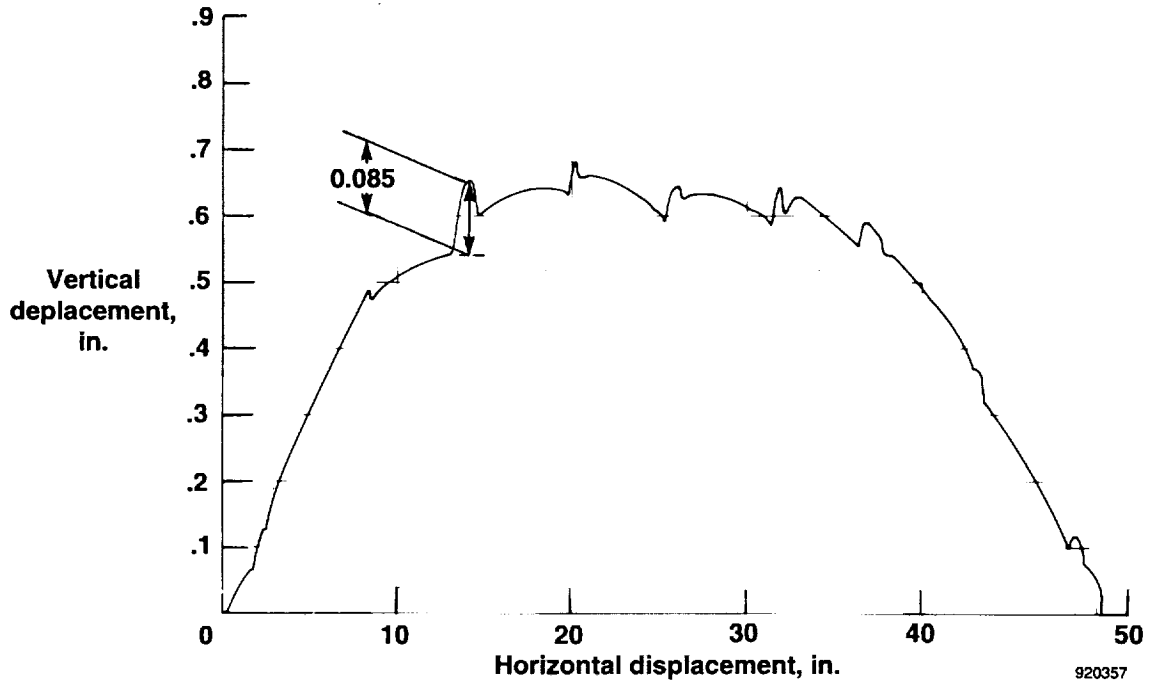


Fig. 19 Thermal protection system tile profilometer trace (landing gear door) (adapted from Ref. 33).

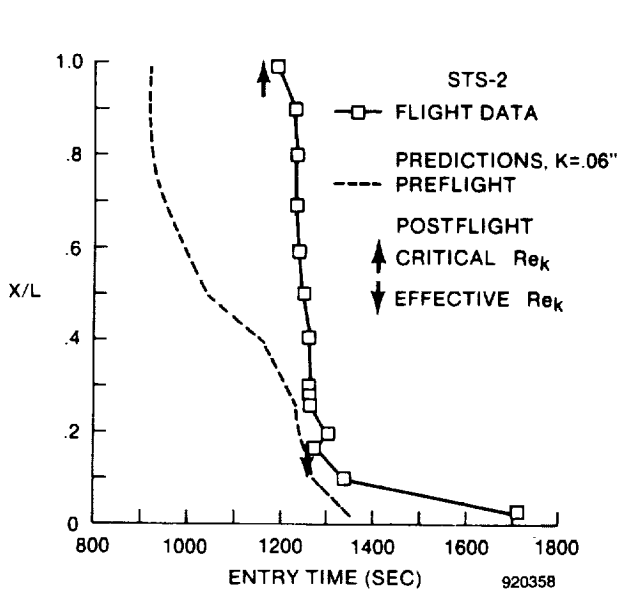


Fig. 20 Comparison of predicted and measured transition times for STS-2 (from Ref. 34).

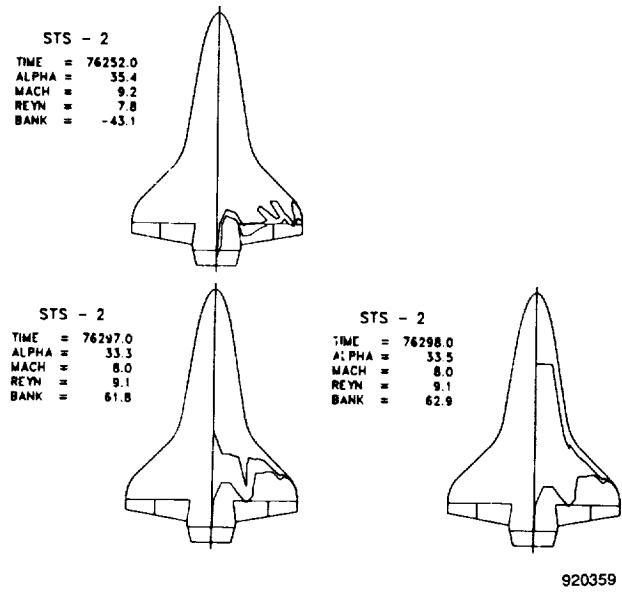


Fig. 21 Three STS-2 transition contour plots (from Ref. 35).

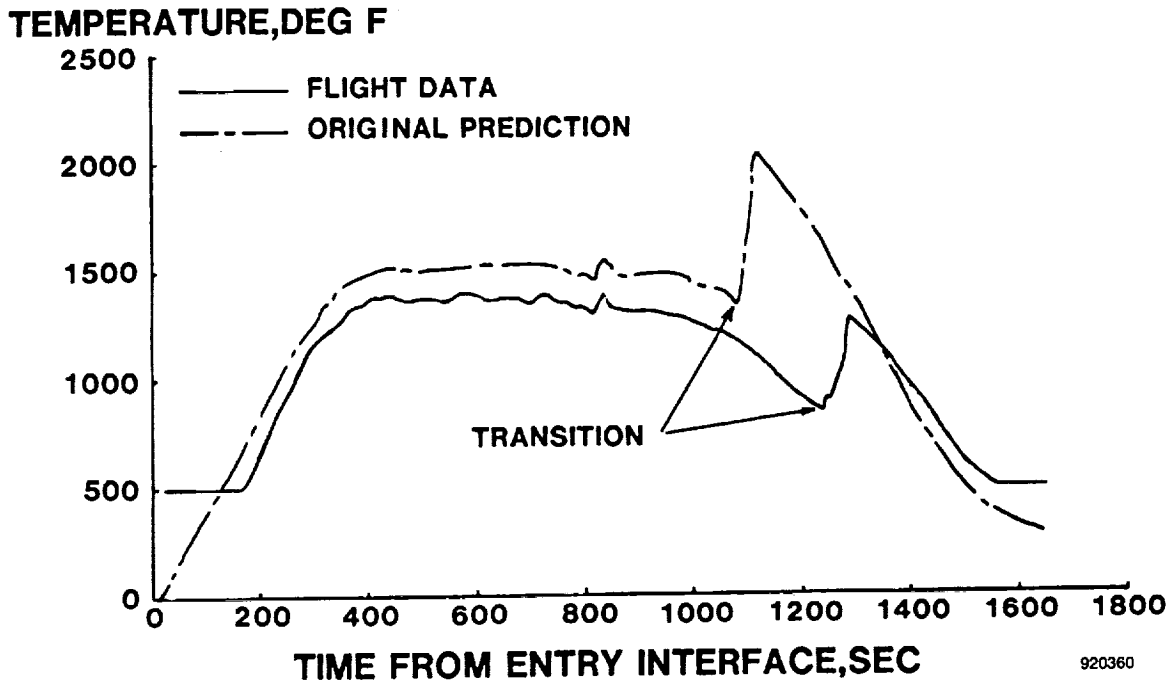


Fig. 22 Lower surface temperature comparison at $X/L = 0.7$ (from Ref. 36).

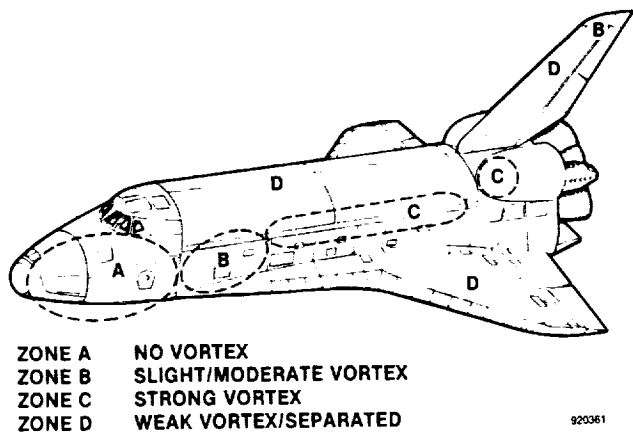


Fig. 23 Fuselage side heating patterns (from Ref. 42).

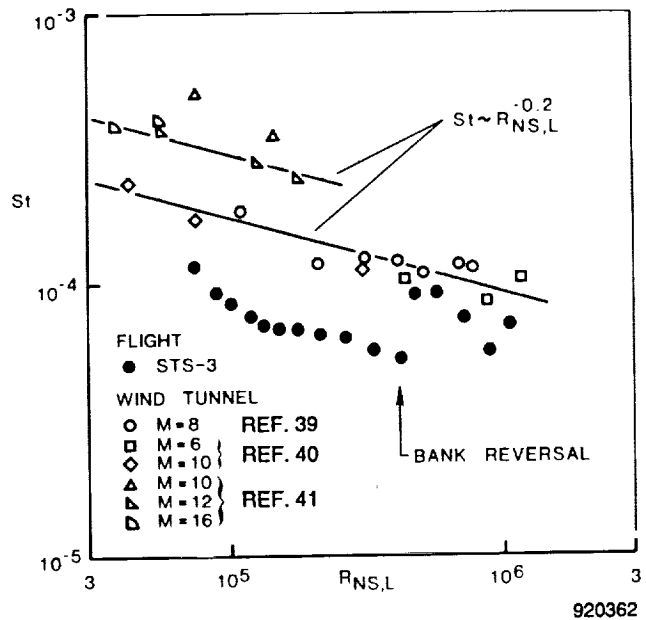


Fig. 24 Stanton number versus normal shock Reynolds number for points on the lee side centerline at $X/L = 0.4$ (adapted from Ref. 38). Solid symbols used for all flight Mach numbers.

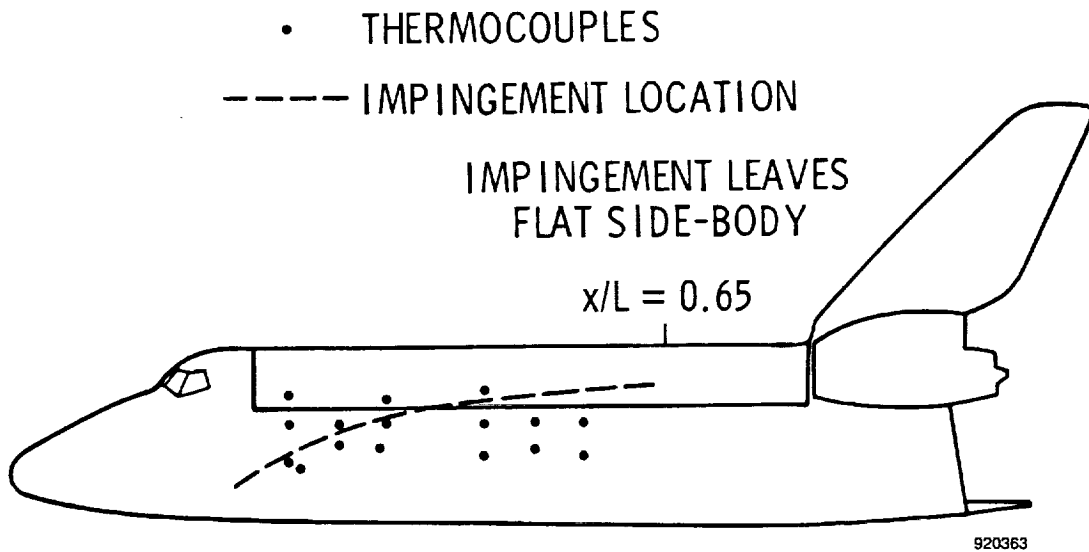


Fig. 25 Predicted location of impingement line with respect to side fuselage thermocouples for a typical reentry condition at $M_\infty = 10.37$ (from Ref. 37).

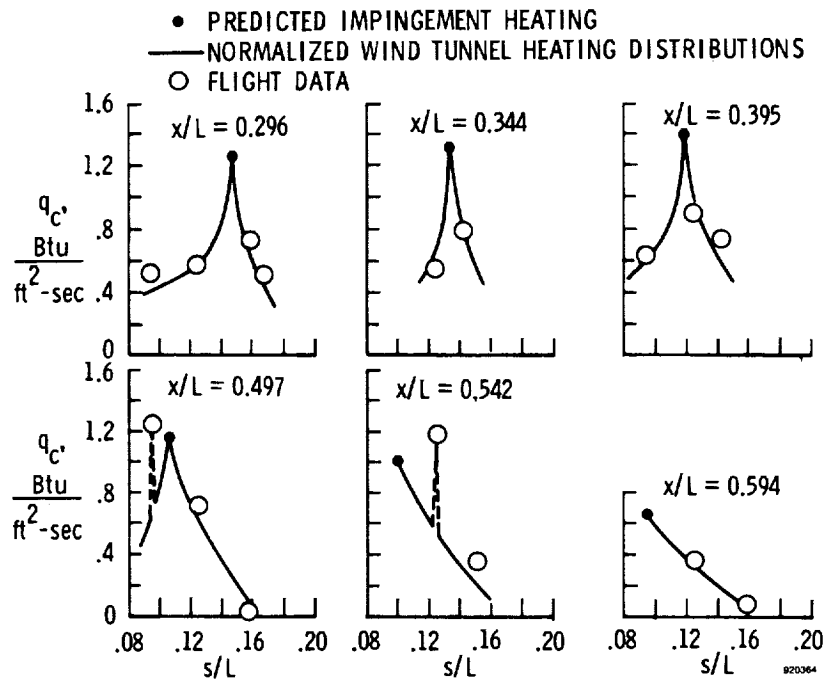


Fig. 26 Comparison of wind-tunnel-heating distributions, impingement-heating predictions, and STS-3 measurements at $M_\infty = 10.37$ (from Ref. 37).

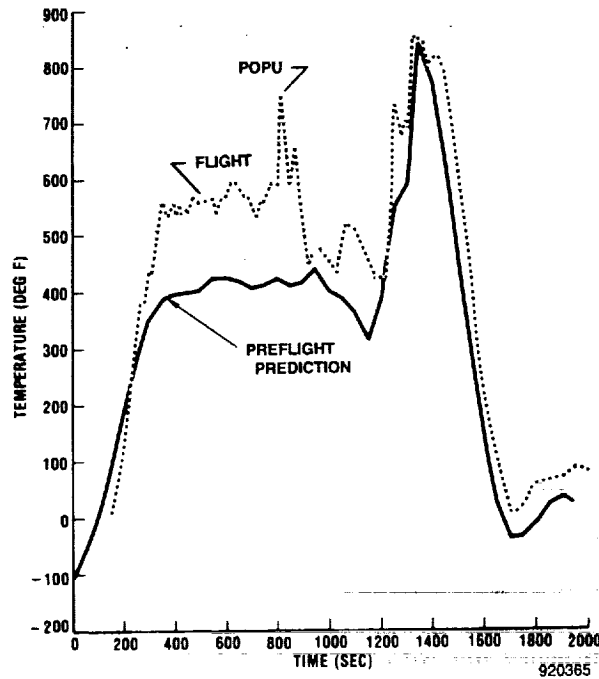


Fig. 27 The STS-2 OMS pod temperature profiles (adapted from Ref. 42).

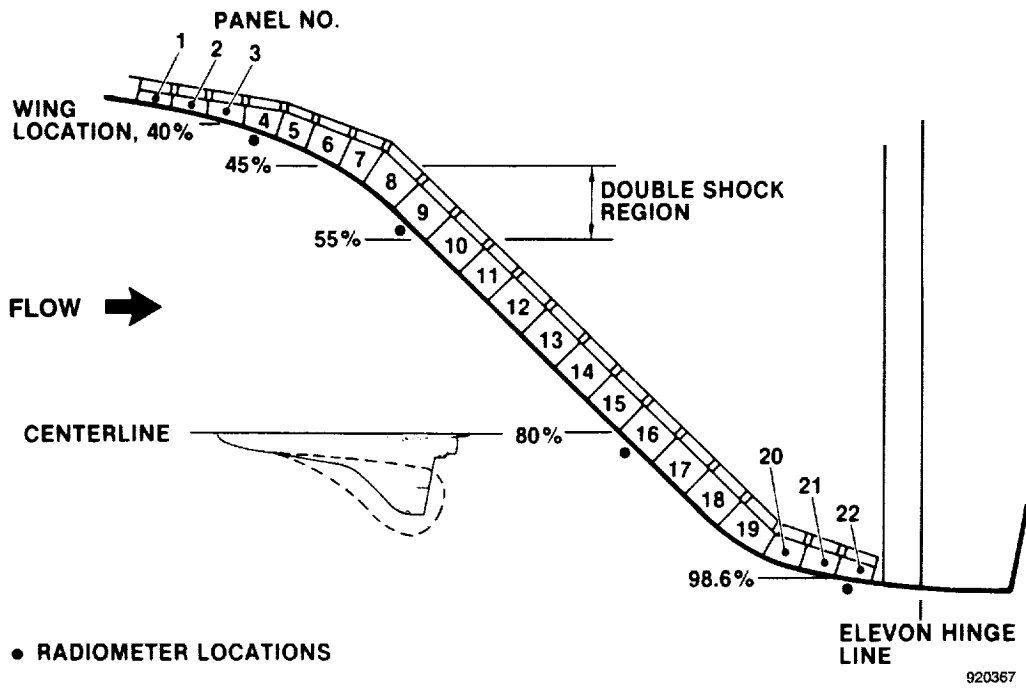


Fig. 28 Orbiter radiometer locations (adapted from Ref. 43).

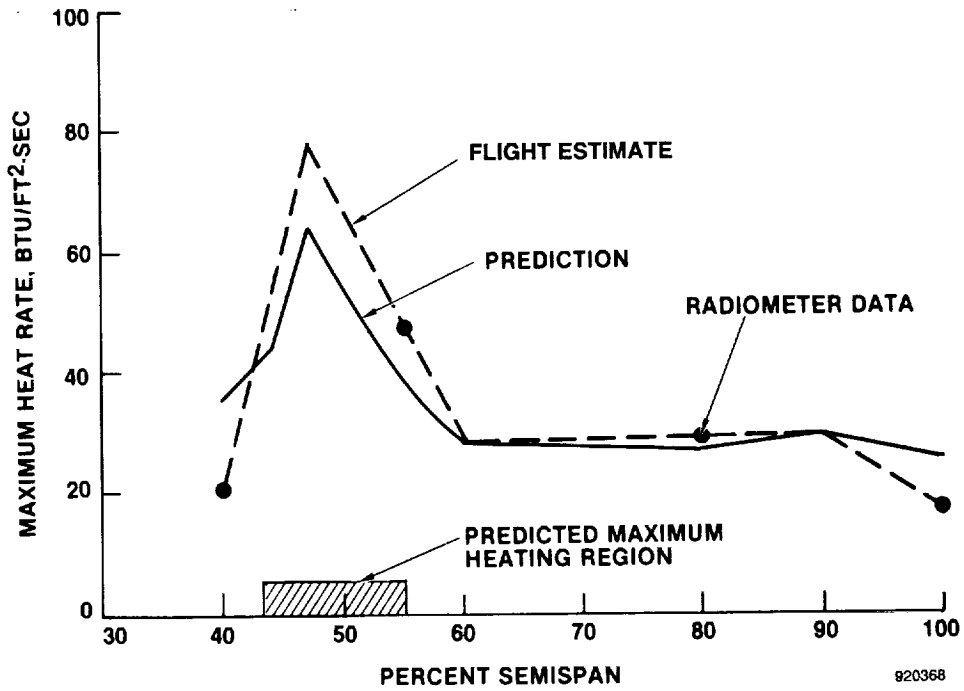


Fig. 29 Spanwise leading-edge maximum heat rate comparison (from Ref. 43).

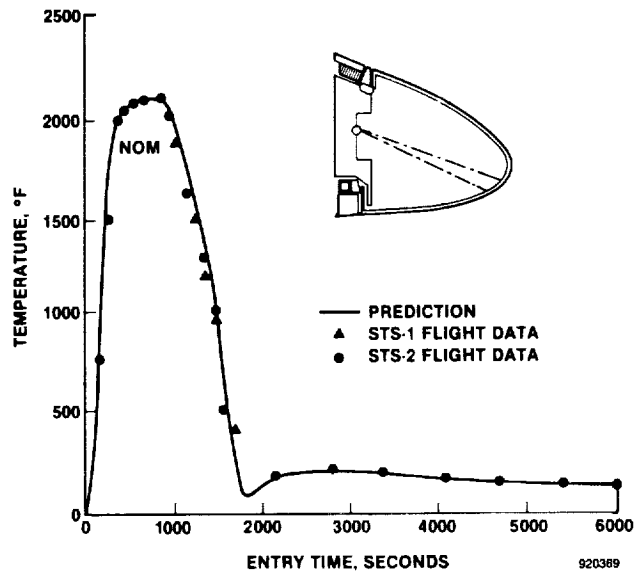


Fig. 30 The 80-percent semispan leading-edge data comparison with prediction (from Ref. 43).

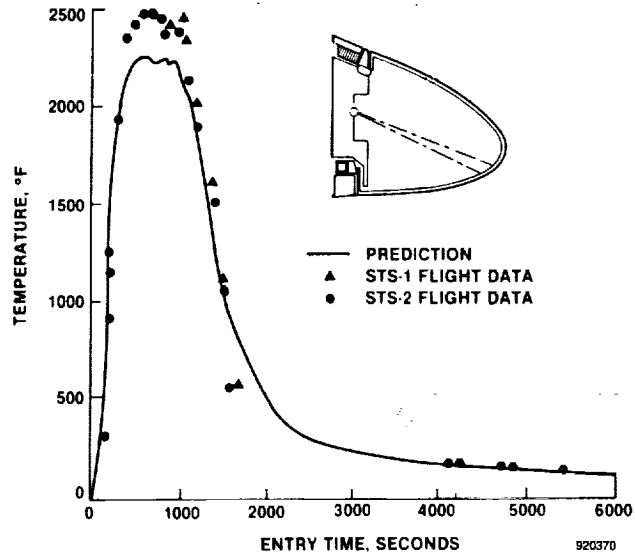


Fig. 31 The 55-percent semispan leading-edge data comparison with prediction (from Ref. 43).

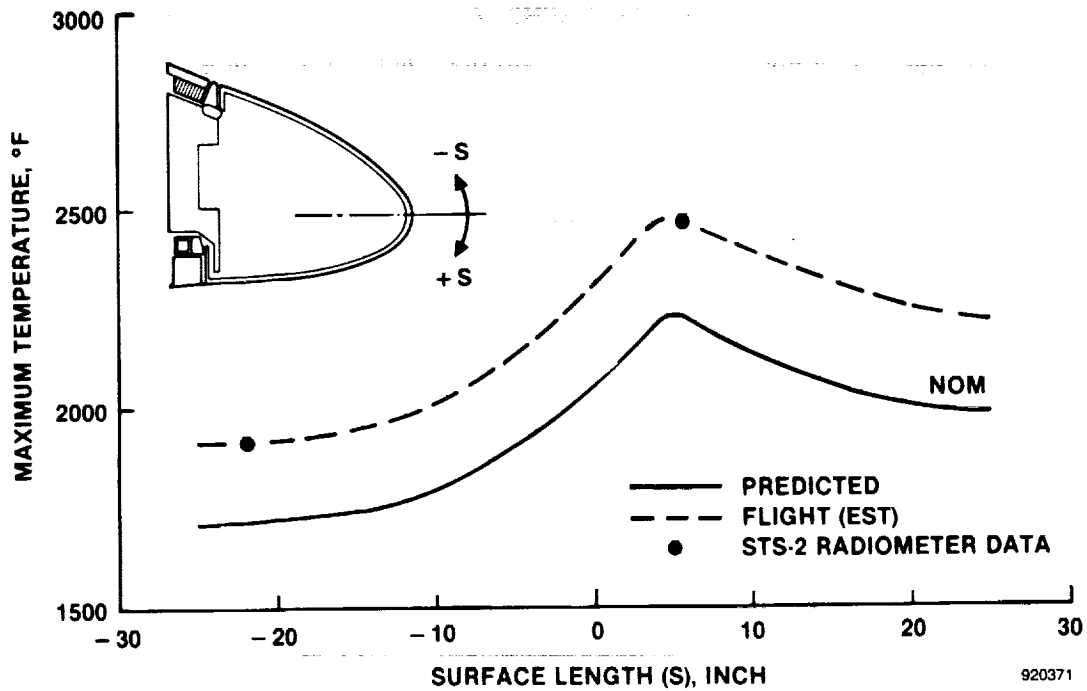


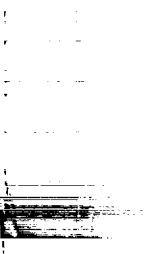
Fig. 32 The 55-percent semispan leading-edge temperature distribution (from Ref. 43).

REPORT DOCUMENTATION PAGE

Form Approved
OMB No. 0704-0188

Public reporting burden for this collection of information is estimated to average 1 hour per response, including the time for reviewing instructions, searching existing data sources, gathering and maintaining the data needed, and completing and reviewing the collection of information. Send comments regarding this burden estimate or any other aspect of this collection of information, including suggestions for reducing this burden, to Washington Headquarters Services, Directorate for Information Operations and Reports, 1215 Jefferson Davis Highway, Suite 1204, Arlington, VA 22202-4302, and to the Office of Management and Budget, Paperwork Reduction Project (0704-0188), Washington, DC 20503.

1. AGENCY USE ONLY (Leave blank)		2. REPORT DATE June 1993	3. REPORT TYPE AND DATES COVERED Technical Memorandum	
4. TITLE AND SUBTITLE Space Shuttle Hypersonic Aerodynamic and Aerothermodynamic Flight Research and the Comparison to Ground Test Results			5. FUNDING NUMBERS WU 506-69-50	
6. AUTHOR(S) Kenneth W. Iliff and Mary F. Shafer				
7. PERFORMING ORGANIZATION NAME(S) AND ADDRESS(ES) NASA Dryden Flight Research Facility P.O. Box 273 Edwards, California 93523-0273			8. PERFORMING ORGANIZATION REPORT NUMBER H-1894	
9. SPONSORING/MONITORING AGENCY NAME(S) AND ADDRESS(ES) National Aeronautics and Space Administration Washington, DC 20546-0001			10. SPONSORING/MONITORING AGENCY REPORT NUMBER NASA TM-4499	
11. SUPPLEMENTARY NOTES Presented as AIAA 92-3988 at the 17th Aerospace Ground Testing Conference, Nashville, Tennessee, July 6-8, 1992.				
12a. DISTRIBUTION/AVAILABILITY STATEMENT Unclassified — Unlimited Subject Category 02			12b. DISTRIBUTION CODE	
13. ABSTRACT (Maximum 200 words) Aerodynamic and aerothermodynamic comparisons between flight and ground test for the Space Shuttle at hypersonic speeds are discussed. All of the comparisons are taken from papers published by researchers active in the Space Shuttle program. The aerodynamic comparisons include stability and control derivatives, center-of-pressure location, and reaction control jet interaction. Comparisons are also discussed for various forms of heating, including catalytic, boundary layer, top centerline, side fuselage, OMS pod, wing leading edge, and shock interaction. The jet interaction and center-of-pressure location flight values exceeded not only the predictions but also the uncertainties of the predictions. Predictions were significantly exceeded for the heating caused by the vortex impingement on the OMS pods and for heating caused by the wing leading-edge shock interaction.				
14. SUBJECT TERMS Aerothermodynamics, Boundary-layer transition, Catalytic effects, Flight-to-ground test correlation, Hypersonic aerodynamics			15. NUMBER OF PAGES 31	
			16. PRICE CODE A03	
17. SECURITY CLASSIFICATION OF REPORT Unclassified	18. SECURITY CLASSIFICATION OF THIS PAGE Unclassified	19. SECURITY CLASSIFICATION OF ABSTRACT Unclassified	20. LIMITATION OF ABSTRACT Unlimited	



Σ

1

2

3

4

5

6

National Aeronautics and
Space Administration
Code JTT
Washington, DC
20546-0001
Official Business
Penalty for Private Use, \$300



POSTMASTER: If Undeliverable (Section 158
Postal Manual) Do Not Return
